Title

In Situ/Operando (Soft) X-ray Spectroscopy Study of Beyond Lithium-ion Batteries

Journal

Energy & Environmental Materials, 4(2)

ISSN

2575-0348

Authors

Yang, Feipeng
Feng, Xuefei
Liu, Y-Sheng
et al.

Publication Date

2021-04-01

DOI

10.1002/eem2.12172

Peer reviewed

Article category: Review

Subcategory: Batteries, soft X-ray spectroscopy

In-situ/operando (soft) X-ray spectroscopy study of beyond lithium-ion batteries

*Feipeng Yang, Xuefei Feng, Yi-Sheng Liu, Li Cheng Kao, Per-Anders Glans, Wanli Yang, Jinghua Guo**

Dr. Feipeng Yang, Dr. Xuefei Feng, Dr. Yi-Sheng Liu, Prof. Jinghua Guo

Joint Center for Energy Storage Research, Lemont, IL 60439, USA.

Dr. Feipeng Yang, Dr. Xuefei Feng, Dr. Yi-Sheng Liu, Dr. Li Cheng Kao, Dr. Per-Anders Glans, Dr. Wanli Yang, Prof. Jinghua Guo

Advanced Light Source, Lawrence Berkeley National Laboratory, Berkeley, CA 94720, USA.

Email: jguo@lbl.gov

Prof. Jinghua Guo

Department of Chemistry and Biochemistry, University of California Santa Cruz, Santa Cruz, CA 95064, USA.

Keywords:

In-situ/operando, (soft) X-ray spectroscopy, beyond lithium-ion battery, interface

Abstract

The lightweight, rechargeable lithium-ion battery is one of the dominant energy storage devices globally in portable electronics due to its high energy density, no memory effect, wide operating voltage, lightweight, and good charge efficiency. However, due to safety concerns, the depletion of lithium reserves, and the corresponding increase of cost, an alternative battery system becomes more and more desirable. To develop alternative battery systems with low cost and high material abundance, e.g. sodium, magnesium, zinc and calcium, it is important to understand the chemical and electronic structure of materials. Soft X-ray spectroscopy, e.g. X-ray absorption spectroscopy (XAS), X-ray emission spectroscopy (XES) and resonant inelastic soft X-ray scattering (RIXS), is an element-specific technique with sensitivity to the local chemical environment and structural order of the element of interest. Modern soft X-ray systems enable operando experiments that can be applied to amorphous and crystalline samples, making it a powerful tool for studying the electronic and structural changes in electrode and electrolyte species. In this article, the application of in-situ/operando (soft) X-ray spectroscopy in beyond lithium-ion batteries is reviewed to demonstrate how such spectroscopic characterizations could facilitate the interpretation of interfacial phenomena under in-situ/operando condition and subsequent development of the beyond lithium-ion batteries.

1. Introduction

As an electrical energy storage device with high energy density, wide operating voltage, good efficiency and no memory effect, lithium-ion battery has dominated the market of portable electronics including mobile phone, laptops and electric vehicles, etc.[1–3] Based on Bloomberg new energy finance, the global light duty passenger electric vehicle market is forecasted to achieve more than 20 million sales globally by 2030. Roughly, 30% of the total

U.S. energy consumption is devoted to transportation while another 40% to electricity generation.[4] To supplant fossil fuels with electricity, portable electrical energy storage devices needs to be more efficient and less in cost. Underlying so much portable modern technology, significant scientific progress has been made in lithium-ion batteries academically and commercially.[1] However, the demand for higher energy densities and lower cost have pushed the lithium-ion batteries near their limits. To make electric vehicles feasible, it is imperative to understand considerably new battery chemistries with higher energy densities than the lithium ion, designated as "beyond lithium-ion" batteries.[2,4–8] Examples include Li-air[9], Li-S[10,11], Na-ion[12–16] batteries, and multivalent-ion batteries including Mg-ion[17–38], Zn-ion[39,40], Ca-ion batteries[17], etc.

Table 1 summarizes the properties of several different beyond Li-ion batteries. The Li-ion batteries have the advantages of high energy density and high voltage but are limited by safety factors and high manufacturing cost corresponding to the depletion of low natural lithium reserve. The Na-ion, Mg-ion, Ca-ion and Zn-ion batteries are lower in terms of cost because of their high abundance but compared with Li-ion batteries, they are suffering from moderate energy density, low capacity, low energy density, and low cell voltage, respectively. [41] In the beyond Li-ion batteries to be introduced, Na-ion batteries are the first alternative because of cost-efficiency, sustainability and safety. However, the Na-ion battery is limited by the development of anode material, as graphite does not allow the intercalation of Na^+ ions.[42] Mg-ion batteries received lots of attention because of the high capacity of Mg metal anode, dendrite-free plating and stripping, and the sustainability and corresponding low cost.[43,44] Ca-ion batteries have lower charge density of Ca^{2+} ions, a similar potential of 0.17 V vs Li, and a similar volumetric capacity of that of Li. The limitations are similar to those of Mg-ion batteries e.g. low diffusion rates of Ca^{2+} ions and high reduction potential.[41,43] Zn-ion batteries offers potential in grid-scale related energy storage[45], but suffers from dendrites formation

and irreversible discharge capacities.[46] In general, the battery research is composed of two electrodes, an oxidant (cathode) and a reductant (anode), and an electrolyte in which ionic components transfer.[47] In the study of ion solvation shell in electrolytes and the charge transfer at the electrode/electrolyte interfaces, both of which notably affect the battery performance and of significant to advance battery research, (soft) X-ray spectroscopy techniques including XAS, XES and RIXS are irreplaceable as they are sensitive to the electronic states of an element of interest, which is affected by its local chemical environment in the electrochemical cycling.

Table 1. Summary, composition, and properties for the different beyond Li-ion batteries.

Battery	Cathode	Anode	Electrolyte composition	Full-cell performance	
				Energy Density (Wh/kg)	Durability (Cycles)
Li-ion battery	$LiFePO_4$	Graphitic carbon	1M $LiClO_4$/EC-DMC	90-120	2000[41]
	$LiCoO_2$		1M $LiPF_6$/EC-DMC	150-240	1000[41]
Na/K-ion battery	$Na_{1.5}VPO_{4.8}F_{0.7}$	Nanostructured carbon	1M NaClO4/ EC0.45·PC0.45·DMC0.1	80-100	120-210[48,49]
	$Na_{0.45}Ni_{0.22}Co_{0.11}Mn_{0.66}O_2$		10 mol% NaTFSI/ $PYR_{14}FSI$	70-110	100[50]
	P′3-type $Na_{0.52}CrO_2$	Metal anode	KTFSI	195	200[51]
Mg-ion battery	Mo_6S_8	Mg (2200)	$Mg(AlCl_2BuEt)_2$/THF	40	2000[44]
	Mg	Mg_2Sn	APC electrolyte	45	150[52]
Ca-ion battery	Carbon-based layered Na_2FePO_4F	C-based layered BP2000 carbon	0.7 M $Ca(PF_6)_2$/EC-DMC-EMC	40-45	300[53]
			$Ca(PF_6)_2$/EC-PC	16-20	50[54]

	Ca_xCuHCF	PANI	$Ca(NO_3)_2$ aqueous electrolyte	70	200[55]
Zn-ion battery	V_2O_5	Zn	3M $Zn(CF_3SO_3)_2$ aq. electrolyte	70-75	4000[56]
	$Co_{0.247}V_2O_5 \cdot 0.94 4H_2O$		Polyacrylamide-based hydrogel	458.7	7500[57]

Synchrotron-based X-ray absorption spectroscopy (XAS)[58–60] measures the X-ray absorption coefficient as a function of photon energy, and is sensitive to the oxidation state, bond length, coordination chemistry for materials in solid, liquid, or gas states with or without long-range ordering.[61] Complementary to that of X-ray powder diffraction (XRD), it is employed in various studies regarding battery materials.[62] Soft XAS, which involves with the excitation of core electron and subsequent decay process, is depicted in Figure 1a. Firstly, a core level electron is excited by the incident photon to the empty electronic state above the Fermi level. Thus, the information provided by XAS is regarding the unoccupied electronic structure, with the existence of core hole. Then, the excited state decays through the fluorescence or Auger channel, emitting photons or electrons, respectively. Approximately, the total fluorescence yield (TFY) and total electron yield (TEY) signals are proportional to the quantity of the core hole created. Because of the different mean free path of electrons and photons in the sample, TEY is surface sensitive while TFY is bulk sensitive, with a probing depth of a few nanometers and several hundred nanometers, respectively. The soft X-ray region (50 eV to 2 keV) covers the 1*s* to 2*p* excitations of low Z elements (e.g. lithium, sodium) and 2*p* to 3*d* transitions of 3*d* transitions metals (e.g., magnesium, zinc, calcium), as it is shown in Figure 1b. The X-ray emission spectroscopy (XES) depicts the intensity vs. energy distribution of the emitted photons, providing information during the decay process of occupied valence electrons that fill the core hole.[63] For resonant inelastic X-ray scattering

(RIXS), the emission spectra strongly depend on the incident photon energies, making it an ideal probe for high correlated electron systems.[64] More importantly, the recent development of high-efficiency RIXS has enabled this powerful tool for studying both transition-metal and oxygen states of the beyond Li-ion battery electrodes.[65,66]

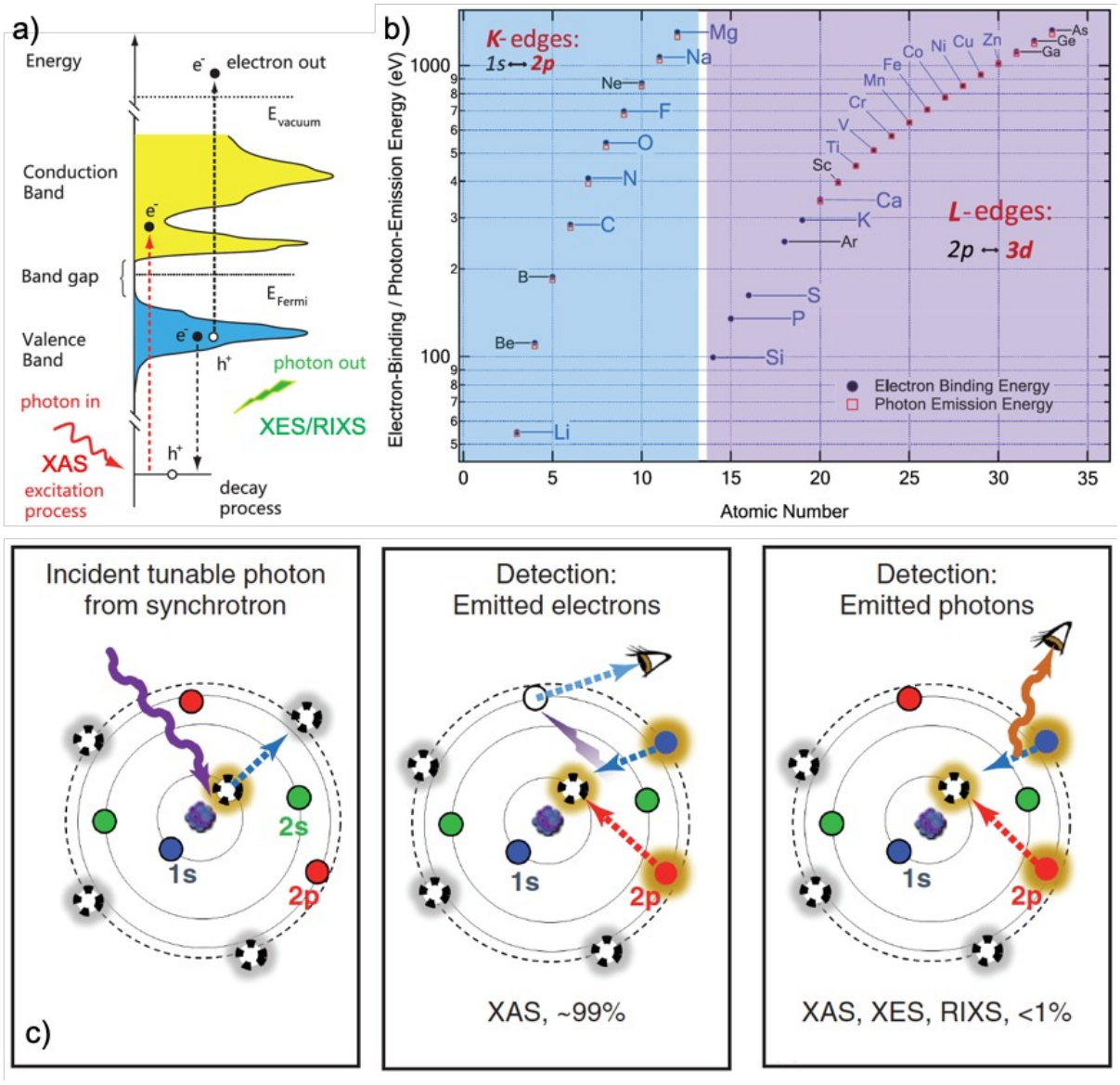

Figure 1. (a) A schematic of soft XAS/XES/RIXS, which involves excitation of core electron and following decay process. (b) Coverage of elements and corresponding excitations that are accessible by soft X-ray spectroscopy (50 eV to 2 keV). K- and L-edge spectroscopy detects the 2*p* and 3*d* states of the specific elements commonly used for batteries, respectively. (c)

Atomic schematic of the core-electron excitation, photon-in-electron-out XAS and photon-ion-photon-out XAS/XES/RIXS. Reproduced with permission.[67,68] Copyright 2016 IOP Publishing Ltd and Copyright 2013 Elsevier.

The discuss below will also include X-ray absorption spectroscopy studies of 3d transition metal K-edge X-ray absorption near-edge spectroscopy (XANES) and extended X-ray absorption fine structure (EXAFS). Although such 3d transition metal K-edge XANES and EXAFS do not fall in the region of soft X-rays (50 eV to 2 keV), they also play an important role in the study of beyond lithium-ion batteries. Such XANES and EXAFS are usually measured in transmission mode, and provide details of the coordinating species, coordination number, distances, and mean square deviations in distances surrounding the element of interest. In addition to comparisons made to standard reference samples, fitting FEFF calculated data from models built with different parameters including ligand type, dopant, distance, and vacancy with the measured data is a common way to analysis the EXAFS spectra.[69]

With respect to battery research, an example is demonstrated how XAS is contributing to the battery binder design.[70] The strategy is to adjust the LUMO energy levels of the binder to let electrons cathodically dope the polymer in-situ. The lowest energy onset of the absorption edge in XAS denotes the LUMO states since the XAS probes the excitation of core electrons to the unoccupied states, as shown in Figure 2a. XAS provides useful information on how functionality of the polymer binder will affect the battery performance, leading to new design strategies of high-capacity anodes. In another important study area of battery, cathode materials, soft XAS is also very useful because most intercalation type cathodes are 3d transition metal (TM) compounds whose L-edge energy range falls in the experimental

window of soft XAS. Such 3d TM electrochemical cycling resulted electronic evolution and structural change is suitable to be probed with soft XAS at TM L-edge, i.e., transition from 2p core level to 3d unoccupied states, providing detailed information on the evolution of electronic states at different chemical stages.[63] As shown in Figure 2b, a sophisticated in-situ soft XAS setup to monitor the electrode electron state during electrochemical cycling empowers the revealing of the charge dynamics in battery electrodes. RIXS is more sensitive compared to XAS to detect subtle chemical contrast at the interface of two chemical species, e.g., the ion-solvation shell in liquid electrolytes (Figure 2c), which is a critical issue in battery systems involved with the charge transfer process.[71] The oxygen K-edge soft XAS spectra do not change much for different concentrations because of the XAS measured here are from the solvent molecule (H_2O) which is the same for pure solvent and that in solvation shells. However, RIXS spectra collected at the 534.2 eV excitation energy observed a significant change which suggests low-energy excitations of vibrational modes in RIXS are significantly suppressed in the ion solvation shell. Detailed ion solvation shell structure can be derived from the analysis of the high resolution RIXS spectra.[72]

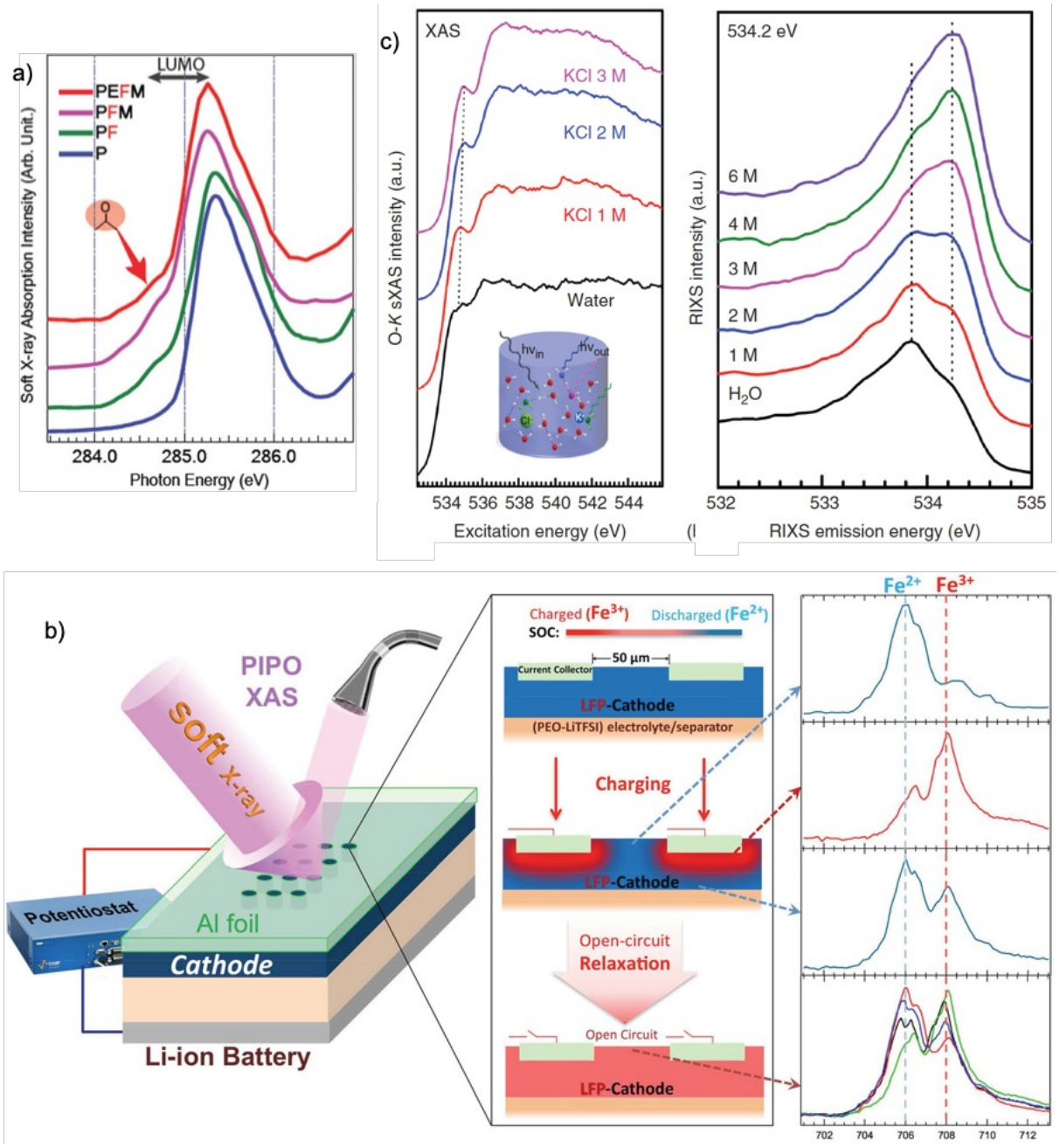

Figure 2. (a) C K-edge XAS spectra of a series of polymer materials as binders in battery. (b) A schematic of in-situ cell for soft XAS measurement and corresponding electrodes in charging/relaxation, and key XAS spectra revealing the state-of-charge (SOC) configurations in-situ. (c) In-situ sXAS and RIXS of an aqueous salt solution with different KCl concentrations. Adapted with permission.[70,72,73] Copyright 2013, 2014 American Chemical Society and Copyright 2013 Nature Publishing Group.

In-situ/operando XAS cells for measuring liquid and gas samples have also been developed to enable probing of interfacial species during the electrochemical charging/discharging process and revealing the non-equilibrium state of the condensed matter interfaces.[74,75] The schematics of the static liquid cell, electrochemical flow liquid cell and gas cell are shown in Figure 3.[74–76] A 100-nm thick Si_3N_4 membrane is used to separate the electrolyte from the ultra-high vacuum (UHV) required to perform soft X-ray experiments. The liquid cells with three electrodes are developed to perform in-situ/operando experiments in which the XAS spectra are collected simultaneously with the voltammetric response of the electrode interface, shedding light on transient interfacial processes.

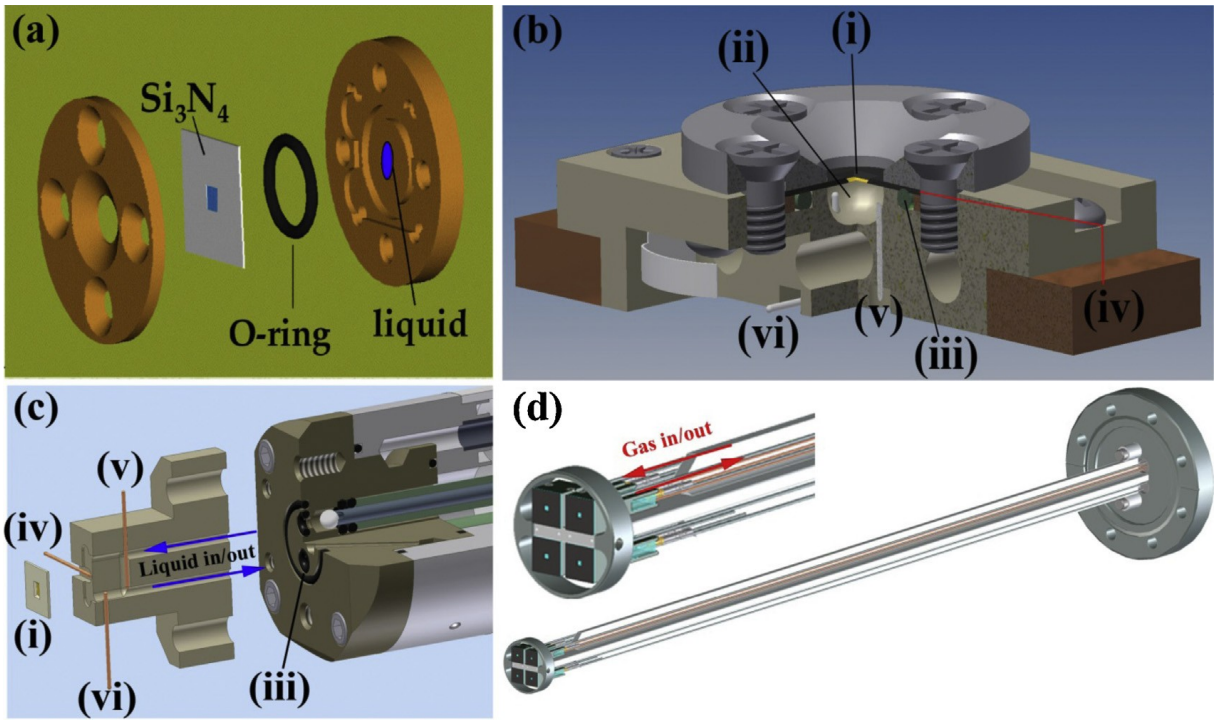

Figure 3. (a) Static liquid cell, (b) electrochemical static liquid cell, (c) electrochemical flow liquid cell, and (d) gas flow cell. Note: (i) Si_3N_4 membrane, (ii) liquid reservoir, (iii) O-ring, (iv) working electrode, (v) counter electrode, and (vi) reference electrode, respectively. Reproduced with permission.[76] Copyright 2015 Elsevier.

Additional core-level X-ray spectroscopies include soft XES, which corresponds to the occupied valence states, and RIXS, which originates from interband and other low-energy excitations, mixed with the noncoherent XES signals.[61]

This article is intended to provide a succinct overview of the recent development of in-situ/operando X-ray spectroscopy and its application in the fundamental and applied research of beyond lithium-ion batteries. A summary of in-situ/operando XAS on various beyond lithium-ion batteries, including Mg-ion[17–38], Zn-ion[39,40], Ca-ion[17], Li-S[10,11], and Na-ion[12–16] batteries, will be discussed in the next section, followed by a brief presentation of several papers employed RIXS and scanning transmission X-ray microscopy (STXM) for applications in the beyond lithium-ion battery field. In addition, a perspective on the future problems to solve with the assistance of in-situ/operando soft X-ray spectroscopies will be discussed.

2. In-situ/operando XAS on beyond lithium-ion batteries

The demand for alternative battery is urgent because of the concern of safety issues, the low abundance of lithium in nature and the depletion of reserve together with the corresponding increase of cost. Compared with lithium (Li), sodium (Na) is abundant in the earth crust, economical, nontoxic, and with a comparable cell voltage, thus Na-ion battery has attracted lots of attention recently, especially in large-scale electrical energy storage applications.[77] For rechargeable batteries based on divalent charge carrier ions such as Mg^{2+}, Ca^{2+}, Zn^{2+}, half the number of ions is needed to achieve the same electrochemical capacity; instead, the capacities will be doubled for the same amount of reacted ions at the electrodes. To expand the electric vehicle range, energy storage systems based on these divalent ions are promising alternatives to Li-ion batteries.[6,44] In this section, a detailed presentation of the involvement of in-situ/operando (soft) XAS in these beyond Li-ion batteries will be presented

with an emphasis on the Mg-ion batteries while other divalent ions batteries, and Na-ion batteries will be briefly discussed.

2.1 In-situ/operando XAS in Mg-ion battery research

Magnesium (Mg) has been used as an anode material in batteries for more than twenty years because of its thermodynamic properties after two breakthroughs.[44] The first was the use of non-Grignard based electrolyte solutions with wide electrochemical windows because Grignard reagents are strong reducing agents and cannot be used in batteries.[78,79] The second breakthrough was the high-rate Mg cathodes based on Chevrel phases.[80] Metallic Mg offers high capacity (3833 mAh/cm^3 vs. 2036 mAh/cm^3 for Li metal) and is naturally abundant and safe due to non-dendritic electrochemical deposition.[81] Being cost effective and environmental friendly, lots of work have been performed and reported in recent years and here in this subsection are a few examples of using (soft) XAS in the study of the electrolyte, anode and cathode in the Mg-ion batteries.

2.1.1 In-situ/operando XAS in electrolyte research

The rate of progress in the rechargeable magnesium batteries is limited by the development of Mg electrolytes because electrolyte transfers ions between anode and cathode in the battery.[82] Complex magnesium organohaloaluminate electrolytes are known to be compatible with the Mg anode allowing for reversible electrochemical Mg deposition and stripping.[83,84] However, while some of these organohaloaluminate salts are stable against electrochemical oxidation, they were observed to be corrosive attributed to the presence of chlorides in their cations or anions.[84] This leads to another type of electrolyte for Mg-ion battery, i.e., Boron-containing electrolytes. A few examples include anions such as $TFSI^-$ and BH_4^-.[18,85]

In 2013, Arthur from Toyota and coworkers studied the effect of electrolytic properties of a magnesium organohaloaluminate electrolyte on magnesium deposition using in-situ electrochemical X-ray absorption spectroscopy. The Mg K-edge was measured by fluorescence on the beamline 6.3.1.2 ISAAS endstation at the Advanced Light Source at Lawrence Berkeley National Laboratory.[34] The X-ray absorption near-edge spectroscopy (XANES) spectra of 0.4 M C_2H_5MgCl-$((C_2H_5)_2AlCl)_2$ electrolyte generated in-situ, the crystallized $[Mg_2(\mu\text{-}Cl)_3{\cdot}6(OC_4H_8)]$ $(AlCl_4)$ solid and 0.4 M $[Mg_2(\mu\text{-}Cl)_3{\cdot}6(OC_4H_8)]$ $(AlCl_4)$ solution in tetrahydrofuran (THF) are shown in Figure 4a. Similar spectral features are observed in (a) peak, (b) shoulder, and (c) broad peak. It indicates the dominant Mg in both the in-situ and dissolved electrolyte is $[Mg_2(\mu\text{-}Cl)_3{\cdot}6(OC_4H_8)]^+$. Extending the in-situ analysis into the extended X-ray absorption fine structure (EXAFS) region, three different potentials, -100, -200 and -400 mV vs. Mg/Mg^{2+} was selected. The -100, -200, and -400 mV stand for before, onset and after electrolyte reduction, respectively (Figure 4b). The EXAFS reveals the presence of a nondimeric and interfacial Mg transient state at potentials below Mg plating. Combined with information from electrochemical transport measurements and XAS including both XANES and EXAFS, a mechanism for Mg deposition in this organohaloaluminate electrolyte is proposed, as it is shown in Figure 4c.

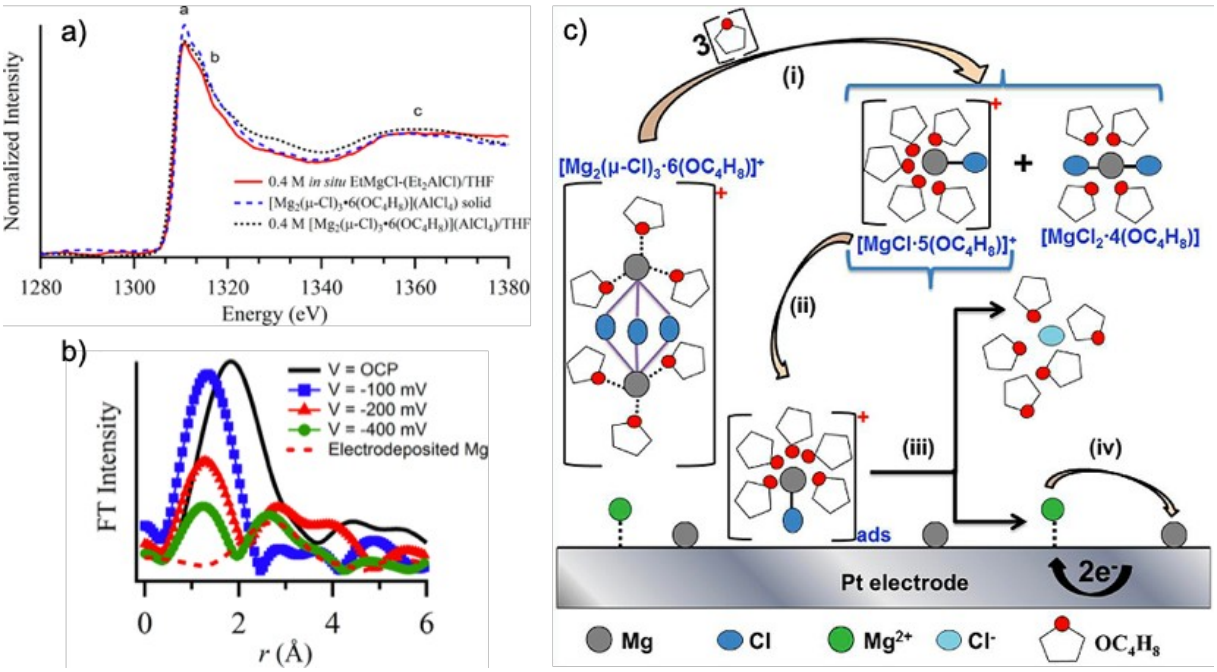

Figure 4. (a) XANES spectra for organohaloaluminate electrolytes. (b) Fourier-transformed EXAFS spectra of the Mg *K*-edge at the Mg metal and electrolyte interface. (c) Proposed mechanism of Mg deposition in organohaloaluminate electrolyte. Reproduced with permission.[34] Copyright 2013 American Chemical Society.

Mizuno et al. also from Toyota investigated the electrode/electrolyte interface in rechargeable magnesium batteries at the same endstation in 2014, focusing on the anode/electrolyte interface.[32] The in-situ observation at this interface offers new insights during Mg deposition on a Pt electrode and during Mg dissolution from the electrochemically deposited Mg metal. In Figure 5a, at -0.1 V vs. Mg, Mg deposition has not started, but the edge observed at 1304 eV indicates a new intermediate species before Mg deposition. The more negative the potential is, the higher the intensity of the new edge and eventually at -0.75 V, the edge of XANES spectrum shifts to 1301 eV, corresponding to metallic Mg. This observation of the new edge reveals the presence of the intermediate species formed at the interface between the organohaloaluminate electrolyte and Mg metal. The reverse process

while applying positive potentials is shown in Figure 5b. Contrary to the scanning electron microscopy (SEM) and X-ray photoelectron spectroscopy (XPS) studies in which a solid-state species was not observed, the XAS indicates an intermediate soluble layer at this Mg/electrolyte interface. A schematic structure of the Mg/electrolyte interfacial layer with this intermediate species $[MgCl{\cdot}5THF]^{+}$ is shown in Figure 5c. This process is faster than expected despite of low transport of properties of Mg-ion in organohaloaluminate electrolyte. This study reveals the intermediate species for the very first time, and further scrutiny using in-situ/operando XAS regarding the solvation-desolvation process at the electrolyte/electrode interface is of fundamental interest and importance to make Mg battery go further beyond lithium-ion batteries.

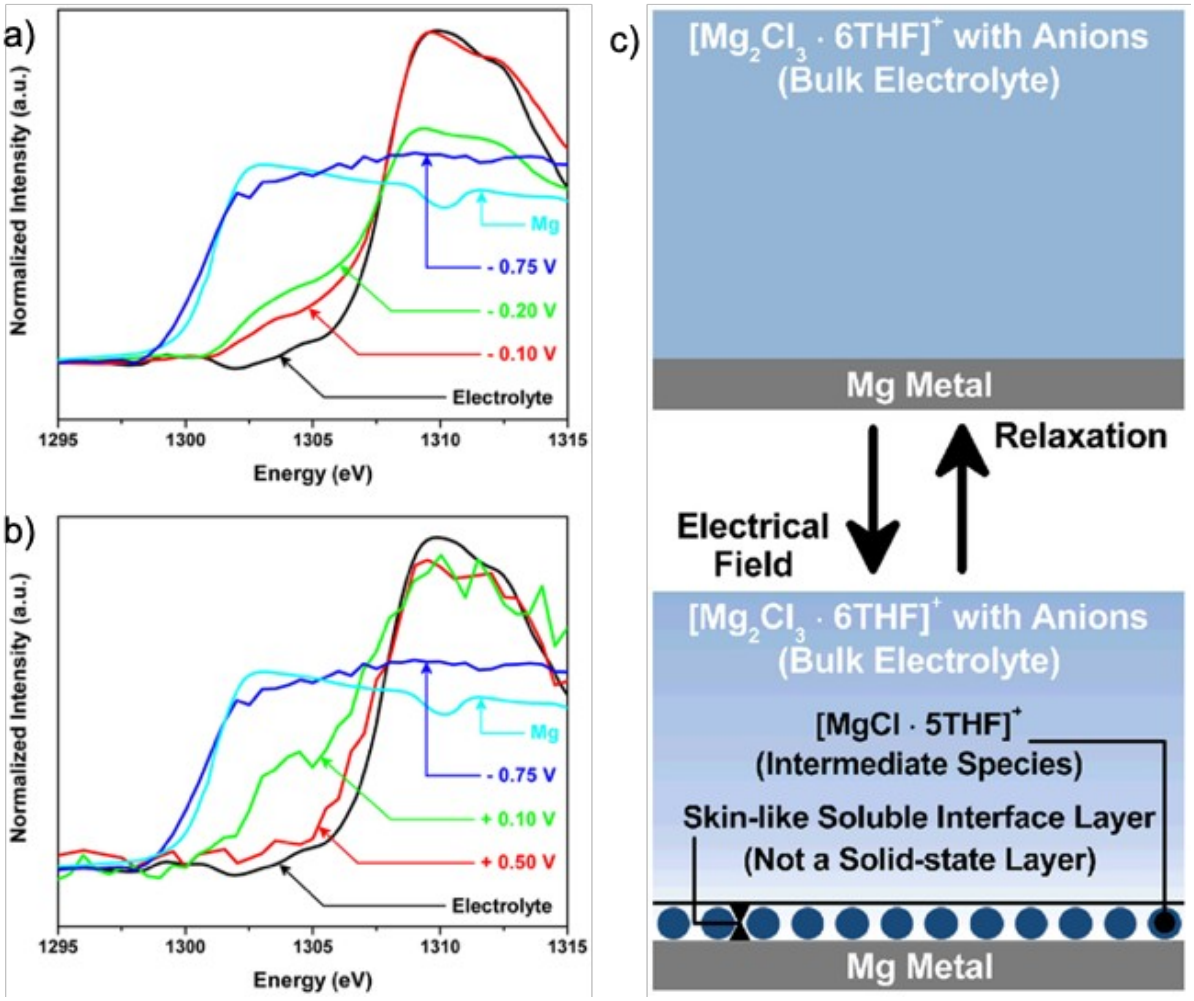

Figure 5. In-situ X-ray absorption near edge structure (XANES) spectra of the Mg K-edge for the interface between Mg metal and the organohaloaluminate electrolyte (a) during Mg deposition on a Pt electrode and (b) during Mg dissolution from the electrochemically deposited Mg metal onto the Pt electrode. (c) A schematic image of the Mg metal/organohaloaluminate electrolyte interface layer incorporating intermediate species. Reproduced from Ref[32]. Open Access article.

Arthur and his coworkers also investigated the boron-containing electrolytes using soft XAS and electrochemical methods.[18,85,86] $Mg(BH_4)_2$ electrolytes enabled reversible Mg plating/stripping attributing to high reductive stability of BH_4^-.[83] With Mg K-edge fluorescence on the beamline 6.3.1.2 ISAAC endstation and complementary operando TEM information, Arthur et al. identifies the active component for the deposition of Mg metal as the contact-ion pair $[Mg(\mu\text{-}H)_2BH_2]^+$, and experimentally proves that the formation of boron clusters accompanied by H_2 gas formation accompany the deposition of Mg, and is critical in the formation of solid electrolyte interphase (SEI) on the Pt surface. With operando Mg K-edge XANES, Mg K-edge EXAFS and B K-edge XANES, the interphase formation from $Mg(BH_4)_2$ electrolytes are revealed, as it is shown in Figure 6. The red peak at 1313 eV and blue peak at 1317 eV represent the similar bulk constituents of the electrolytes in different concentrations, and the green peak at 1307 eV is the deposition of Mg species onto the electrochemical interface. In the deposition of metallic Mg surface (iia) and interaction of anion (iib) are the vital steps, that promote the reductive formation of H_2 (iii) gas and higher order boron clusters (iv).

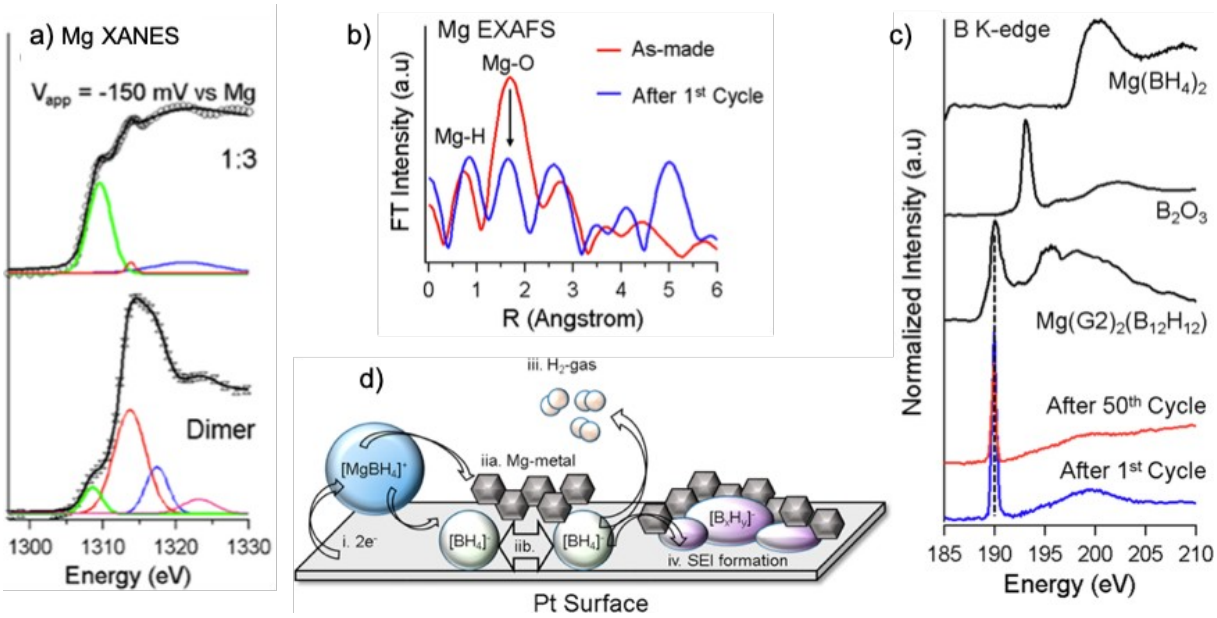

Figure 6. (a) Mg K-edge XANES of the cell under operando V = -150 mV vs. Mg applied to the interface. The solid black line is the fit obtained from the addition of the red, blue, green and purple peaks. (b) Mg K-edge EXAFS of 1:3 Mg:Li borohydride electrolyte as-prepared and after the first reduction/oxidation cycle. (c) B K-edge XANES after the 1st cycle and 50th cycle of deposition/dissolution of Mg from 1:3 Mg:Li borohydride electrolyte. (d) A schematic of the interphase formation from $Mg(BH_4)_2$ electrolytes. Reproduced with permission.[18] Copyright 2017 American Chemical Society.

A very recent work through tuning a conventional electrolyte, $Mg(TFSI)_2$ with a $Mg(BH_4)_2$ cosalt in diglyme, highly reversible Mg plating/stripping with a high coulombic efficiency is achieved by neutralizing the first solvation shell of Mg cationic clusters between Mg^{2+} and $TFSI^-$ and enhanced the reductive stability of free $TFSI^-$. The Mg K-edge XANES spectra in this work shows an obvious shift to the low-energy edge for the cell using electrolyte with BH_4^- but not for the cell using electrolyte without BH_4^-. As shown in Figure 7, the pre-edge shift of the Mg K-edge is largely associated with the active Mg cation clusters involved with absorbed BH_4^- at the interface between Pt and electrolyte before Mg

electrodeposition. The charge-transfer process with adsorption of Mg cation clusters involving BH_4^- is identified as the key mechanism for Mg plating and stripping by the in-situ/operando soft XAS in this work at beamline 8.0.1.4, wet-RIXS endstation at ALS using the static liquid cell.

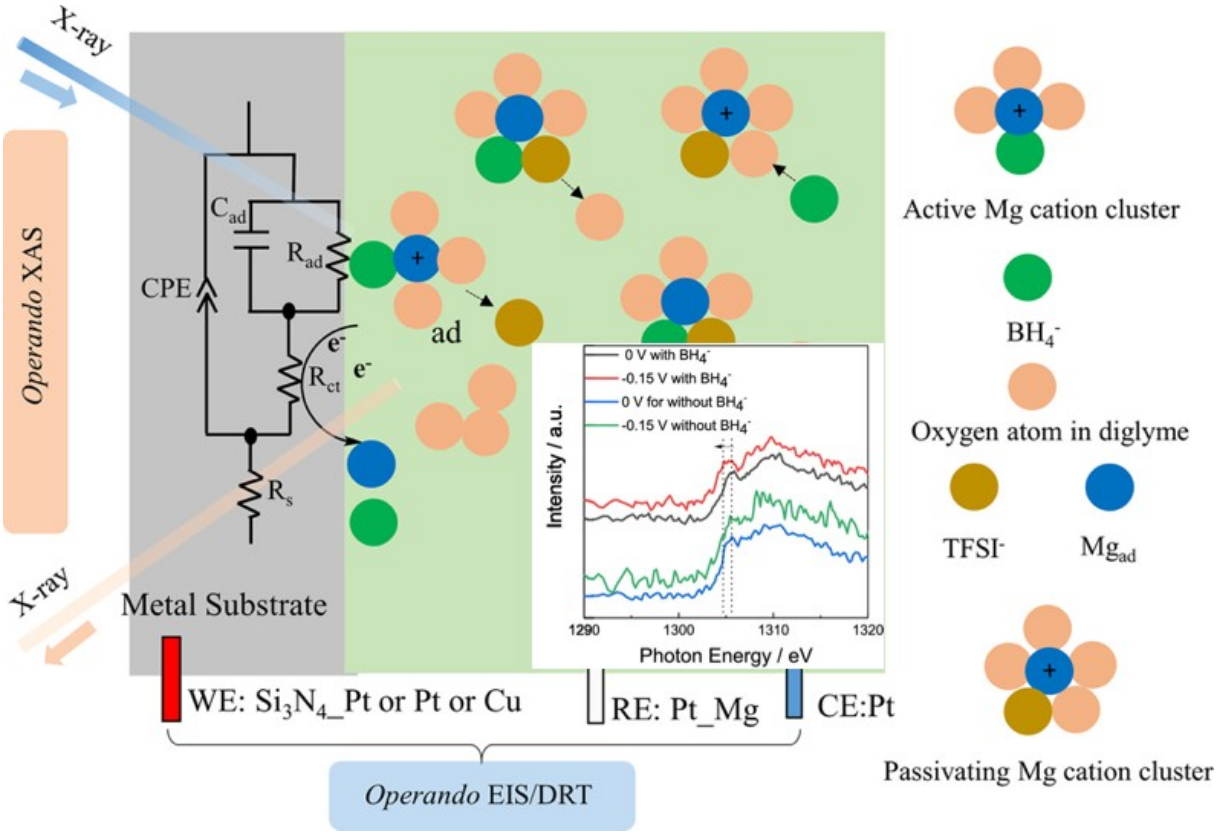

Figure 7. A schematic illustration of probing the electrified interface involving adsorption of active Mg cation clusters and the in-situ/operando Mg K-edge XANES spectra collected using this setup. Reproduced with permission.[22] Copyright 2020 American Chemical Society.

Additional work on the electrolyte of Mg-ion battery was reported. For example, the $Mg(BH_4)_2$ coordination chemistry and the effect of ligands were investigated with that in different solvents, e.g. dimethoxyethane (DME), diglyme (DGM), and THF.[85] Based on the observations, a new electrolyte was developed based on $Mg(BH_4)_2$, diglyme and $LiBH_4$

additive. Such an electrolyte exhibit ~100% coulombic efficiency, cycling stability, and no dendrite formation. Another electrolyte reported recently is inspired by the hydrogen storage properties of $Mg(BH_4)_2$ electrolytes, in which the magnesium monocarborane, $Mg(CB_{11}H_{12})_2$, salt was synthesized.[86] As a simple type of salt compatible with Mg metal with >99% coulombic efficiency, 3.8V vs. Mg high anodic stability, and non-corrosive nature, $Mg(CB_{11}H_{12})_2$ is suitable for future Mg batteries. A very recent work reported the probing of non-equilibrium state of condensed mater interfaces and interfacial dynamics transient processes using operando XAS which runs the CV and collects spectra simultaneously.[87] This work enables to dynamically record interfacial reactions probing the non-equilibrium state of the electrode interface through XAS measurement.

In short, the in-situ/operando XAS plays a significant role in Mg-ion electrolyte research. The operando condition makes it possible to observe the transient state, from which the Mg deposition mechanism is proposed, and the TEY signal enables the revealing of intermediate species at the electrode/electrolyte interface, assisting in the understanding of the charge-transfer process in the Mg plating and stripping. The Mg coordination chemistry information derived from in-situ/operando XAS also assists in the design of new electrolyte with higher coulombic efficiency and no dendrite formation.

2.1.2 In-situ/operando XAS in cathode research

Selective cathode materials with high operating voltage and specific capacity, fast and reversible kinetics of Mg^{2+} migration, and good cycling stability are also the key component of rechargeable magnesium batteries.[82] Lacking of high-voltage cathodes has become a major obstacle on the path to make a complete Mg battery. In this section, the employment of (soft) X-ray absorption spectroscopy in the research of cathode materials, including the

breakthrough Chevrel phase Mo_6S_8, layered materials, polyanionic compounds, spinel structure oxide, and Prussian blue analog (PBA) electrode will be discussed.[28,36,88–90]

As a major breakthrough in the Mg-ion battery cathode, the Cheverel phase, Mo_6S_8, has been used since its first demonstration.[44] As shown in Figure 8, theoretical prediction regarding the charge compensation mechanism of the Chevrel phase is different from most transition metal compounds as the charge transfer occurs on the anions rather than the transition metal center.[90] Mo K-edge and S K-edge XAS studies of the charged (demagnesiated) and discharged (fully magnesiated) Mo_6S_8 samples is used to confirm the theory since it is sensitive to both the electronic structure and the coordination chemistry. During magnesiation, 1) the Mo K-edge XANES presents no red-shift of the absorption edge, which validate that there is no reduction; 2) the pre-edge signature feature becomes more prominent in the S K-edge XANES, attributing to the filling of electronic states at the Fermi level. Such XANES evidence justifies the understanding of Chevrel phase as an important category of Mg-ion battery cathode.

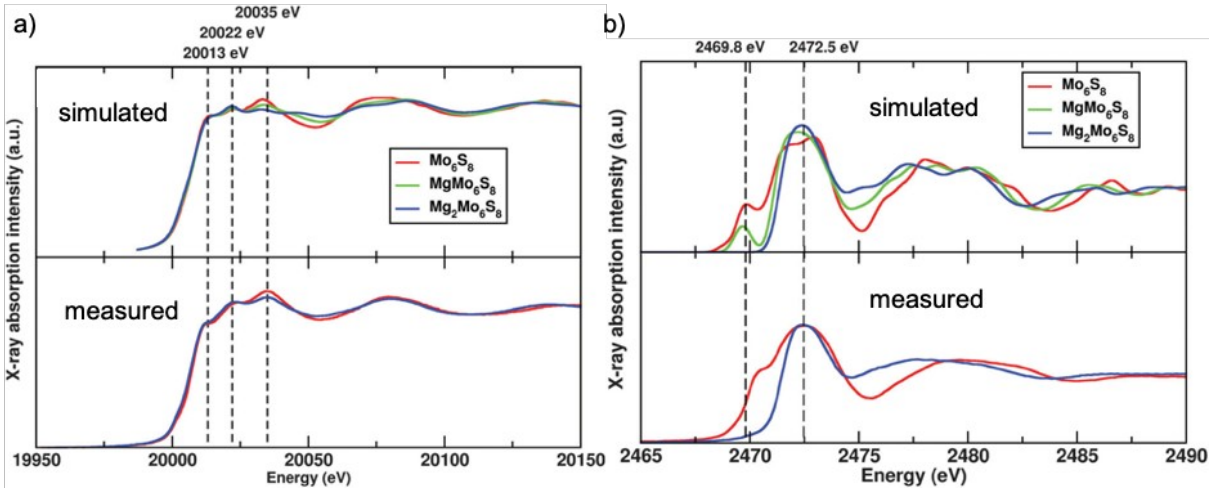

Figure 8. (a) Mo K-edge, (b) S K-edge XANES for various $Mg_xMo_6S_8$ (x=0, 1, 2) samples from simulation and experiment. Reproduced with permission.[90] Copyright 2016 American Chemical Society.

The layered material provides 2D transmission channels while providing insertion sites for Mg^{2+} ions. Following the work of α-MnO_2 in 2012[91], Arthur and coworkers investigated the electrochemical mechanism of K-αMnO_2 as a high energy density cathode for Mg-ion batteries, Mn L-edge soft XAS provides surface sensitivity when using the TEY mode.[33] For samples with various depths-of-discharge, the Mn L-edge soft XAS was calculated and compared with the measurements. With additional information from microscopic techniques, a conversion reaction mechanism is proposed, as opposed to the typical intercalation mechanism in Li-ion batteries. Arthur et al. also deciphered the role of vanadium and phosphorus in the amorphous V_2O_5-P_2O_5 cathodes with the V L-edge XAS by comparing the electronic structure of the V 3d levels in the V_2O_5-P_2O_5 vs V_2O_5 cathodes.[29] With addition of the P_2O_5, a new peak is observed. Increasing to 75:25 mol%, there is a convergence of the V L_3 peaks, while beyond a 25 mol% of P_2O_5, there is a divergence of the L_3 region to separate peaks together with the presence of a new peak. With the variation in the V_2O_5:P_2O_5 ratio, the change in the XAS spectra linked to the P_2O_5 has been validated. Another study of the V_2O_5 nanowire was reported by Fu et al. very recently using in-situ/operando XAS combined with in-situ/operando diffraction techniques.[88] The operando cell and the XAS spectra collected during the first discharge-charge process is shown in Figure 9. With complementary information from XPS, the in-situ/operando XAS validated the reduction/oxidation of V during the Mg insertion/extraction for the first time. In other types of layered material, e.g., TiS_2, the fast kinetics of $MgCl^+$ cations were probed by Mg K-edge soft XAS and S K-edge XAS.[23] The Mg K-edge soft XAS confirmed the intercalated $MgCl^+$ maintain tetracoordination of Mg with 1 Cl and 3 S atoms, while the S K-edge XAS confirmed the sulfur coordination chemistry changed upon $MgCl^+$ intercalation, reflected by several signature spectroscopic features performed on $(MgCl)_xTiS_2$ for x=0, 0.5 and 1.

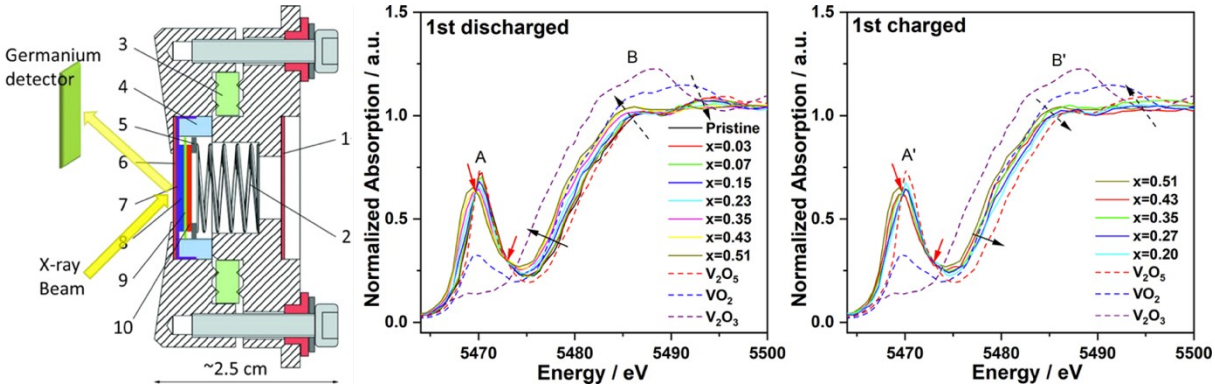

Figure 9. A schematic diagram of the in-situ/operando cell and the operando XANES for the V K-edge during the first discharge-charge process. The isosbestic points are indicated by red arrows. Reproduced with permission.[88] Copyright 2019 American Chemical Society.

In the study of polyanionic compounds, an olivine-type $MgMSiO_4$ (M = Fe, Mn, Co, or Ni) is promising to have high Mg-ion diffusivity because the olivine-type structure in $LiFePO_4$ has a 1D path.[92,93] Such a polyanion compound, Mg_xMnSiO_4, was studied during the charge processes using Mn K-edge XANES, from which the oxidation state of Mn could be derived.[94] The Mn K-edge EXAFS reveals an increase of local structural distortion of Mn-O bonds during charging attributing to Jahn-teller effect of oxidized Mn^{3+} ions. This work inspired the use of nanocrystalline $MgMnSiO_4$ and $MgCoSiO_4$ magnesium metal silicates as Mg-ion battery cathodes, and improved the specific capacities significantly.[31] Similar work to study the olivine-type Mg_xFePO_4 (x= 0-0.4) at the Fe K-edge were reported very recently.[95,96] In Figure 10a, the edge according to the Fe 1s to Fe 4p and to the continuum state was identified for $FePO_4$.[97] With increasing of inserted Mg^{2+}, the XANES shifted to lower energy region, implicating the Fe ions in $FePO_4$ were reduced. In Figure 10b, the XANES shifted back to higher energy region with Mg^{2+} extraction, validating the Fe ions were oxidized. To overcome the degradation of $FePO_4$ during Mg-ion insertion/extraction, highly defective

$FePO_4$ which does not cause secondary phase formation is promising and studied with EXAFS, as shown in Figure 10c and 10d. XANES was also used in the probing of another polyanionic compound $Na_3V_2(PO_4)_3$ cathode in a Mg-Na hybrid battery, and confirmed the changes of V oxidation state in the $Na_3V_2(PO_4)_3/NaV_2(PO_4)_3$ samples and the V atoms are reversible in this redox reaction.[30]

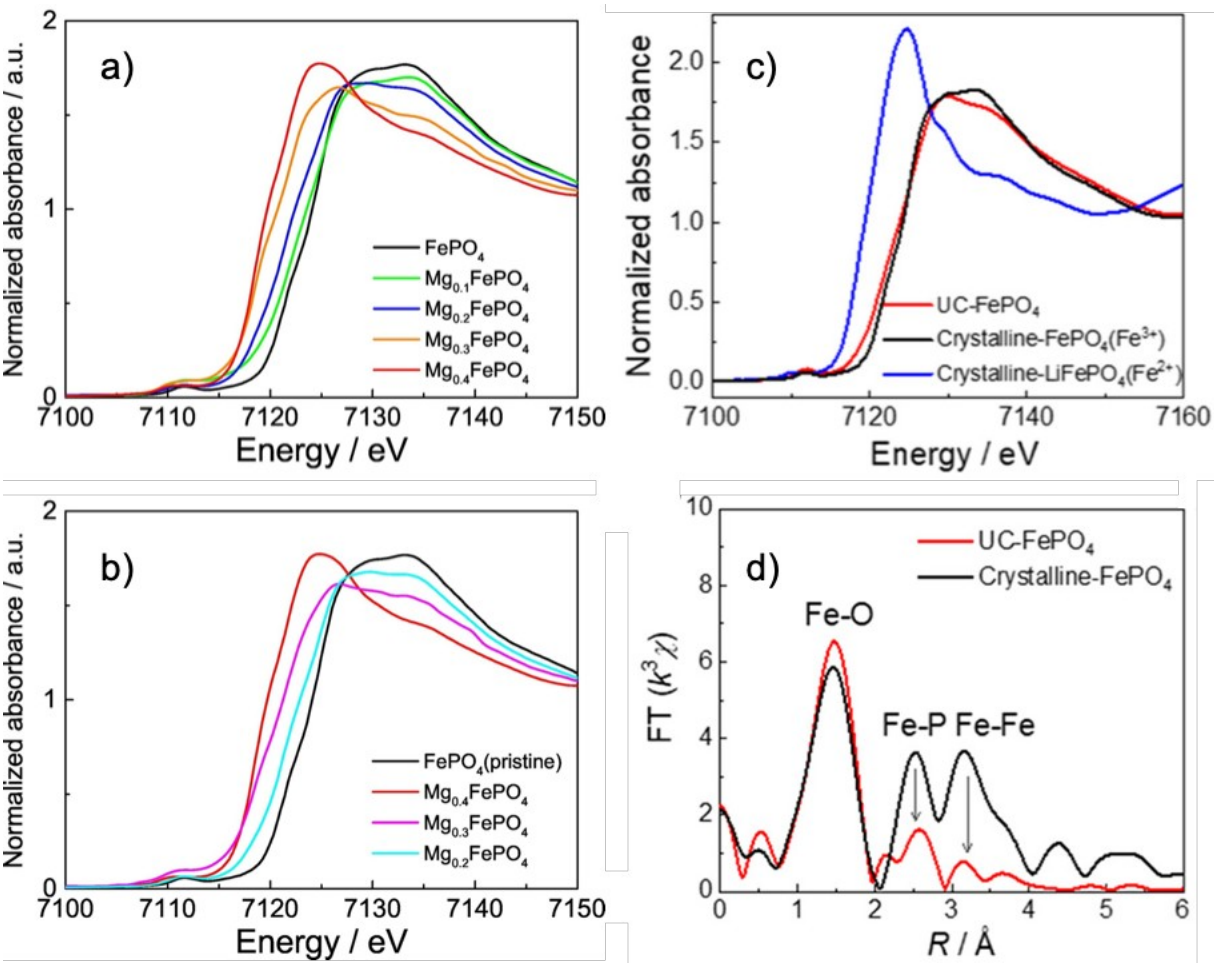

Figure 10. XANES spectra of Mg_xFePO_4 (x = 0-0.4) at the Fe K-edge after magnesium ions (a) insertion and (b) extraction reactions. (c) Fe K-edge XANES spectra of highly defective $FePO_4$, crystalline $FePO_4$, and crystalline $LiFePO_4$. (d) Fourier transform magnitudes from EXAFS oscillation at the Fe K-edge of highly defective $FePO_4$ and crystalline $FePO_4$. Reproduced with permission.[95,96] Copyright 2020 American Chemical Society.

The spinel oxide with high working voltage and stable 3D ion migration pathway is also a promising cathode candidate for Mg-ion batteries. XAS also contributed in an $Mg(Mn_{1-x}Fe_x)_2O_4$ spinel oxide study. The Mn K-edge shifts to lower energy upon discharge and halfway back to higher energy after charging, and the Fe K-edge shifts to lower energy after discharge and completely back to its initial position after recharge. Such changes implicate the charge compensation is realized by variation of the oxidation state change of the Mn(II)/Mn(III) redox couple in the $Mg(Mn_{1-x}Fe_x)_2O_4$ spinel oxides.[25] In another Zinc-based spinel cathode study, XAS spectra measured after discharge/charge were used to validate the valence states of Ni and Co.[28]

Prussian blue analog (PBA) electrodes with 3D open channels for ion diffusion and interstitial sites also benefit from XANES.[36] The Ni K-edge with a slight reduction at the edge energy implicates a reduction of the Ni oxidation state, originating from the Ni redox potential being outside the stability window of the electrolyte. A substantial change in the white line for Mg charged sample is because of the Ni being in a more symmetric coordination environment.[98] As shown in Figure 11, the Fe K-edge also shift with the state of charge of the electrodes. The removal of Na results a 0.5 eV shift to higher energies, indicating 0.5 electron is transferred.[99] During discharge, for Mg, Zn and Ca samples, the edge shifts back to where it was for the uncycled state, revealing the Fe oxidation state is reduced by 0.5. XANES used in this PBA electrode study contribute to a better understanding and practical implementation of the full cell interactions not only in Mg battery but also Ca and Zn batteries.

In summary, the (soft) X-ray absorption spectroscopy has been employed in deciphering the cathode materials, including the magnesiation mechanism of the cheverel phase Mo6S8, the reduction/oxidation of V during the Mg insertion/extraction. It also inspires the use of nanocrystalline magnesium metal silicates as Mg-ion battery cathode to improve

the specific capacities in the study of polyanionic compounds. For the spinel oxide and PBA electrode studies, XANES validates the valence states and coordination chemistry, contributing to both a fundamental understanding and the practical implementation of the full cell interactions.

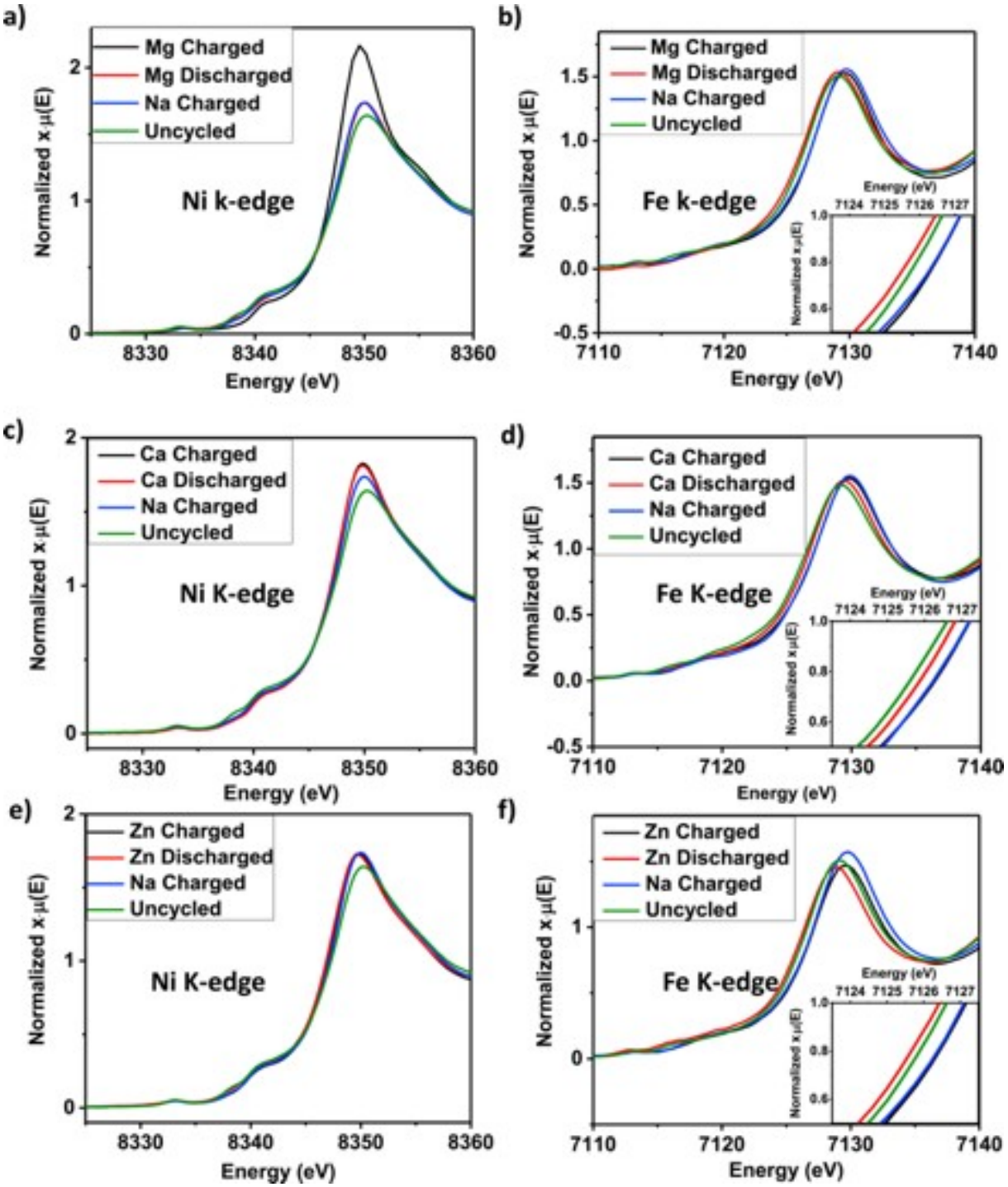

Figure 11. XANES spectra for a,b,c) the Ni K-edge and d,e,f,) the Fe K-edge for the PBA electrode at various states of charge and with Mg, Ca and Zn as insertion ions. Reproduced with permission.[36] Copyright 2016 Elsevier.

2.1.3 In-situ/operando XAS in anode research

Compared with Li, Na, and Ca, the Mg metal could be used directly as an anode since it is less sensitive to the atmosphere and dendrite-free in the recharging process. However, a passivation layer is usually formed which insulates the Mg-ion migration. Thus alloy-based anode to reduce the formation of passivation layers is of significance in current Mg-ion battery anode studies.[82] Inspired by the first published work using bismuth (Bi) with low reduction/oxidation potential and antimony (Sb) with the high theoretical capacity in Mg-ion battery[27,80], a microsized Bi sample was studied with Bi L_3-edge XANES spectra in which the energy inflection point of the L_3-edge implicates the average oxidation state of Bi. A full picture of the origin of the enhanced reversible capacity is validated, which in turn benefited the anode design of a potassium-ion battery as reported recently.[100]

2.2 In-situ/operando XAS in Zn and Ca battery research

The Zn-ion batteries are advantageous over the Li-ion batteries attributing to the high abundance and large-scale production of Zn, non-toxicity nature, low redox potential (-0.76V vs standard hydrogen electrode (SHE)), and stability in H_2O.[101] In a study of the Zn/bilayered hydrated V_2O_5 by Johnson et al.[39], a rechargeable battery using a nonaqueous acetonitrile (AN)-$Zn(TFSI)_2$ electrolyte with a BL-V_2O_5 cathode was investigated using the V K-edge XANES to probe reduction/oxidation of V on cycling as an indicator of Zn ion intercalation and V reduction. The oxidation state is derived by comparing the sample with VO_2 and orthorhombic V_2O_5 standards. All three electrodes exhibit an edge step between V^{4+} and V^{5+}

reference samples, validating the reversibility of the Zn-ion intercalation. A 20% intensity variation of the peak in the pre-edge near 5470 eV is observed, attributing to the distorted square-pyramidal bonding in V_2O_5[102], and the intensity becomes smaller as the local V symmetry increases. In a separate study of Zn batteries, a hydrogen-substituted graphdiyne (HsGDY) is designed as an artificial interface layer and probed with XANES with varying etching depth (0-10 nm) to confirm its chemical characteristics. The peaks at 285.1 eV, 292.9 eV, 285.6 eV and 288.6 eV correspond to the π and σ excitations of the benzene ring, alkynyl and C-O bond, respectively. The distinctive peak at 290.4 eV is a signature of C-H bond and an exclusive feature of HsGDY and being less in GDY, which determines the formation of a giant hexatomic ring served as a natural Zn^{2+} ion tunnel as is shown in Figure 13.[40]

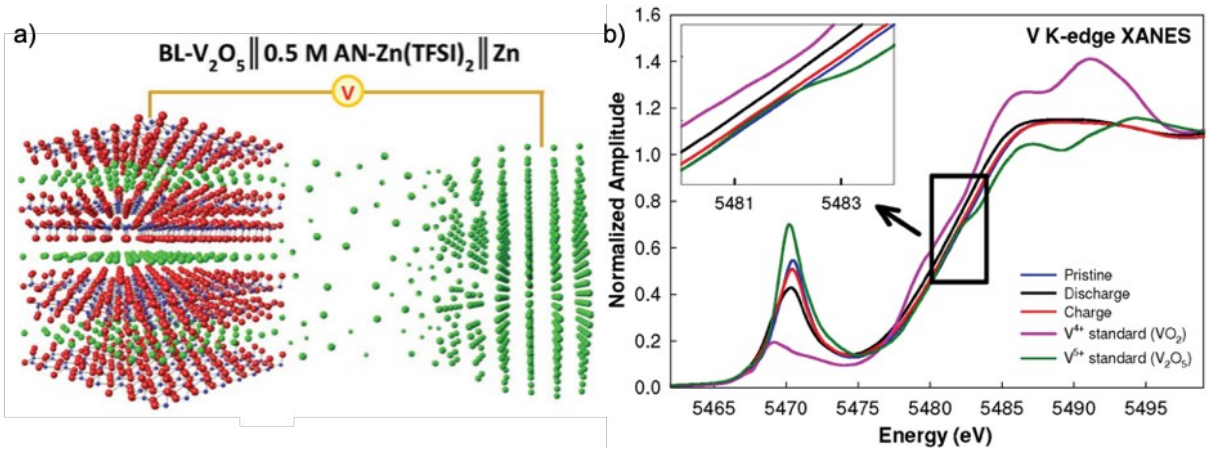

Figure 12. (a) A schematic diagram of Zn/BL-V_2O_5 cell. (red: oxygen, green: zinc, blue: vanadium). (b) Normalized V K-edge XANES for pristine, discharged, and charged BL-V_2O_5 in comparison with two vanadium standards, VO_2 and orthorhombic V_2O_5. Reproduced with permission.[39] Copyright 2016 WILEY-VCH Verlag GmbH & Co.

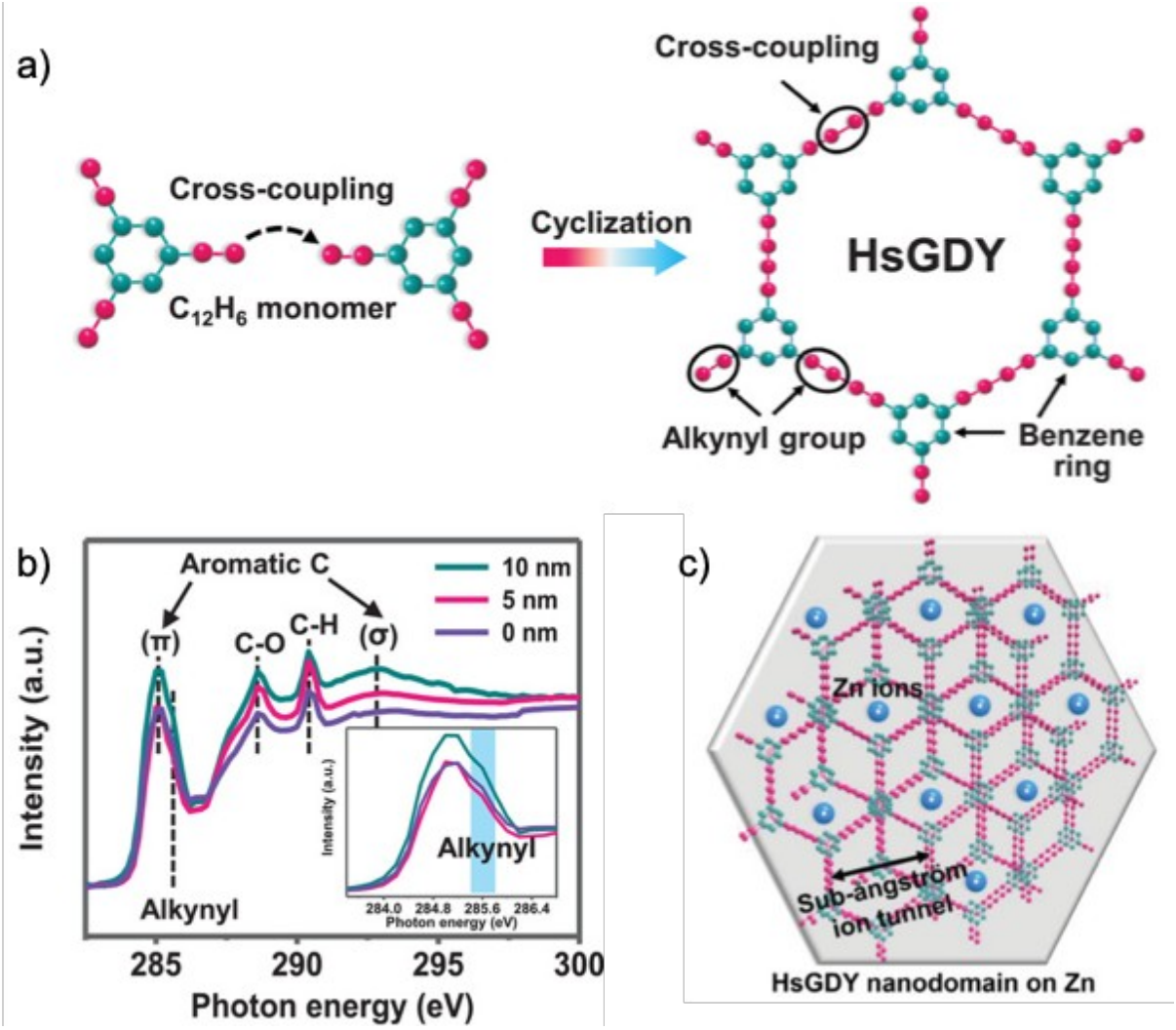

Figure 13. (a) A schematic illustration of the graphdiyne (GDY) and hydrogen-substituted graphdiyne (HsGDY). (b) C K-edge XANES of Zn@HsGDY with different etching depth. (c) A schematic drawing of the sub-ångström ion tunnel of HsGDY. Reproduced with permission.[40] Copyright 2020 WILEY-VCH Verlag GmbH & Co.

The progress on Ca-ion battery is slower compared to that of Mg-ion battery, limited by a breakthrough in Ca plating electrolyte to make the battery reversible.[103] It came recently by the work from Wang et al. demonstrating the reversible Ca electrodeposition at room temperature in $Ca(BH_4)_2$/THF electrolyte.[104] A systematic study of the effect of liquid solvation environment on the electrodeposition is performed by Zavadil et al. very recently

combining DFT simulations, electrochemical methods, Raman and EXAFS.[17] Zavadil and coworkers found the reversible electrodeposition is significantly influenced by the dication charge density and polarizability. The EXAFS spectrum of $Ca(BH_4)_2$/THF are significantly different from $Ca(BHFIP)_2$/THF in terms of both amplitude and phase (Figure 14a). Based on DFT calculations, the differences originate from the changes in oxygen coordination around the Ca^{2+} ion and introduction of Ca-BH_4 coordination. A distinct feature in the real component of the Fourier transform is identified around 4 Å between the electrolyte of $Ca(BH_4)_2$/THF and $Ca(BHFIP)_2$/THF (Figure 14b). There are solid evidence for the presence of multimers in the $Ca(BH_4)_2$ solution. A reaction pathway is proposed based combining the information from both simulation and experiments, as it is shown in Figure 14c. Very recently, Guo et al. and coworkers reported a study of the solvation shell structures of Ca^{2+} in aqueous and organic solutions through a combination of XAS, MD and DFT calculations.[105] The use of the flow liquid cell allows electrochemical potentials to be applied which shows implications in probing transient state species at the interface which can only be observed under in situ/operando conditions. Calcium L-edge XAS spectra for different concentrations of $Ca(BH_4)_2$ in H_2O and methanol solutions were compared in Figure 15a and Figure 15b. The two main peaks and two smaller peaks are 3d electrons in t_{2g} symmetry and 3d electrons in e_g symmetry, respectively. The intensity of the peaks is inversely correlated with the $CaCl_2{\cdot}2H_2O$ concentration in H_2O while the intensities are similar for different concentrations of $CaCl_2{\cdot}2H_2O$ in methanol. Potentials ranging from -0.6 V to +0.4 V were applied on the working electrode while TEY was being collected, and their differences were compared in Figure 15c and Figure 15d. Interestingly, when negative potentials are applied, a_2, b_2 peaks intensities are always larger compared to electrolyte with no potential applied, and the smaller the absolute applied potential, the larger the intensity. Such variations are because of the electrostatic interactions between the working electrode and the Ca^{2+} cations in aqueous

solutions. The results indicate that the interface between liquid electrolyte and solid electrode can be different when electrochemical bias is applied. The TEY surface-sensitive signature makes it one of the very limited techniques that enable probing of such interfaces in future battery studies.

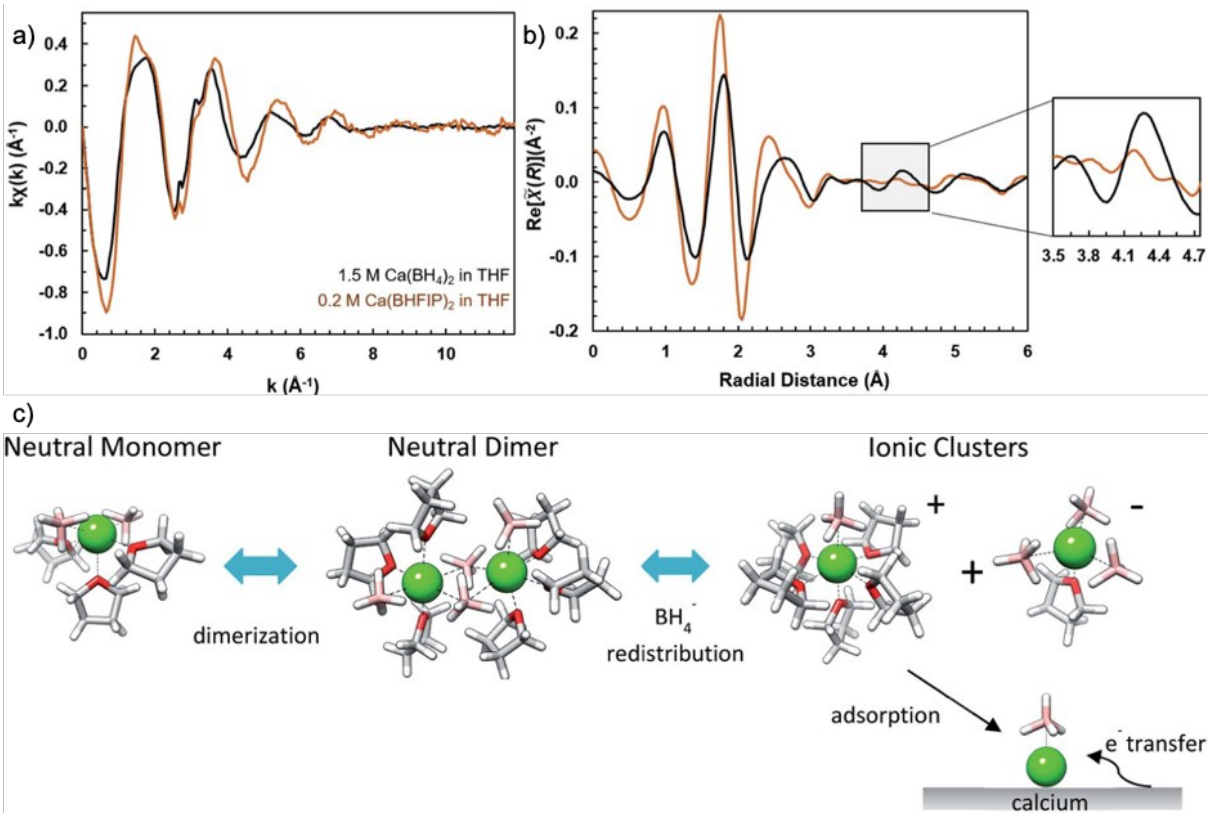

Figure 14. EXAFS spectra of Ca^{2+}/THF electrolytes. A comparison of the k^1-weighted $\chi(k)$ (a) and Re[$\chi(R)$] spectra (b) for the Ca K-edge of 1.5 M $Ca(BH_4)_2$ (black trace) and 0.2 M $Ca(BHFIP)_2$ (orange trace) in THF. (c) Reaction pathway for ionic cluster formation in the $Ca(BH_4)_2$/THF electrolyte yielding $CaBH_4^+$ responsible for Ca electrodeposition. Reproduced with permission.[17] Copyright 2020 The Royal Society of Chemistry.

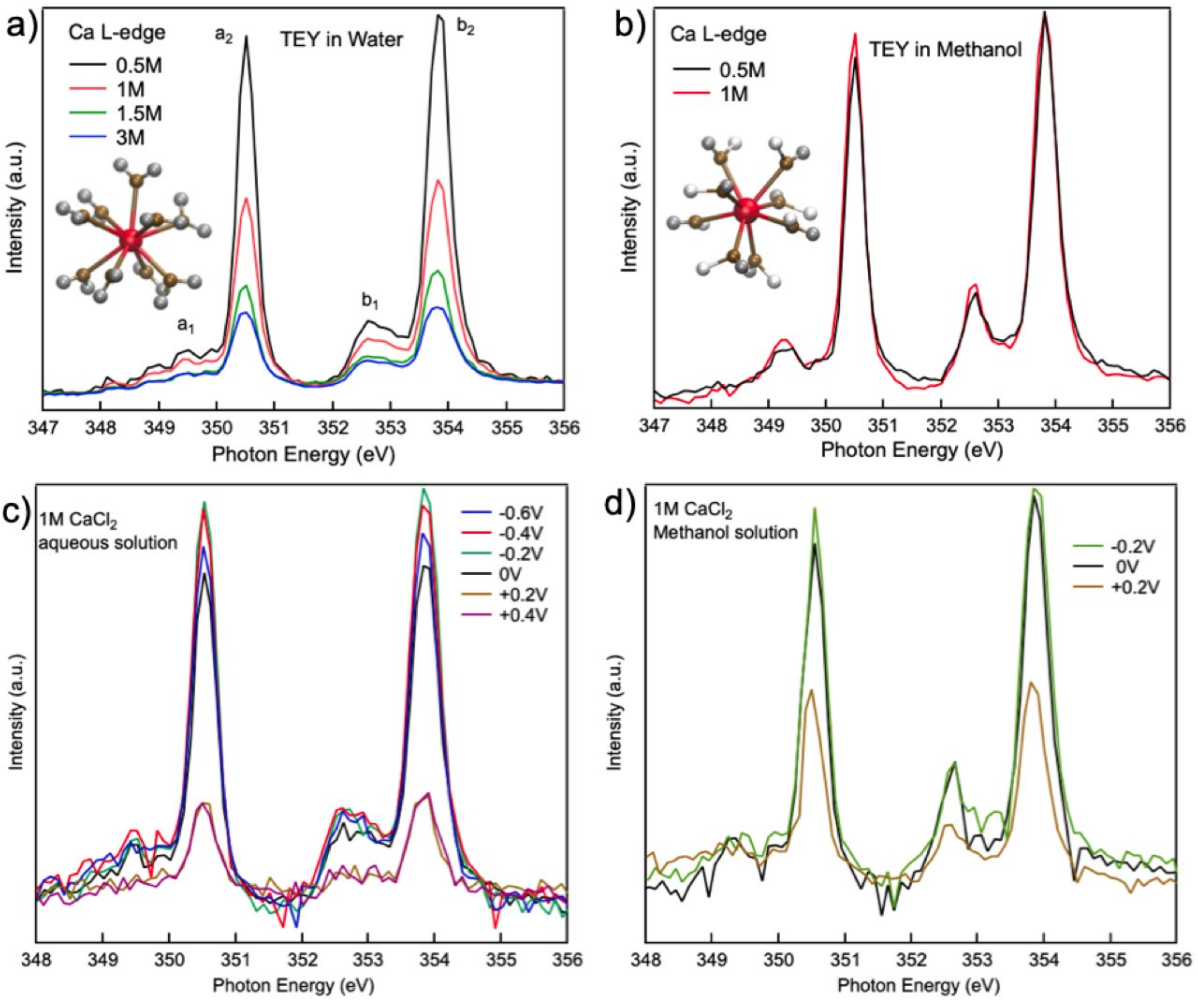

Figure 15. Calcium L-edge TEY mode XAS spectra for (a) 0.5 M, 1.0 M, 1.5 M and 3 M $CaCl_2{\cdot}2H_2O$ aqueous solutions; (b) 0.5 M, 1.0 M $CaCl_2{\cdot}2H_2O$ methanol solutions. In-situ/operando XAS spectra from 1 M $CaCl_2{\cdot}2H_2O$ (c) aqueous and (d) methanol solutions with different potentials applied on the working electrode. Reproduced with permission.[105] Copyright 2020 The Royal Society of Chemistry.

2.3 In-situ/operando X-ray spectroscopy in Na and K battery research

Sodium (Na) battery is another important type of beyond lithium-ion battery attributing to the depletion of lithium source and corresponding increase cost of lithium. Similar properties chemically, three orders of magnitude larger abundance, similar mechanism and similar preparation process compared to Li-ion battery made Na-ion battery a

promising alternative as a beyond lithium-ion energy storage system.[42,106] In a study conducted by Wang and coworkers, XANES was combined with in-situ/operando transmission X-ray microscopy (TXM) to visualize the phase transformation and 2D morphological evolution in the first charge/discharge process.[15] Figure 16a describes the TXM-XANES chemical phase mapping for the selected area during the first discharge cycle. The average XANES in the circled area (Figure 16a) is depicted in Figure 16b. The Ni absorption K-edge variation during the solvation is enlarged in the inset of Figure 16b. The calculated average composition (x in per unit cell) is derived through linear fitting, as shown in Figure 16c. The x value vs the state-of-charge of the battery exhibit monotonic relationship with slight nonlinearity, suggesting a nonhomogeneous reaction mechanism. Through similar analysis, a homogeneous reaction mechanism in the first desodiation process. Wang et al. attributes this interesting phenomenon to the inner crack formation in the sodiation process from which more surface area is provided for the homogeneous desodiation reaction. Additionally, these new cracks will also consume more sodium ions in the first discharge cycle. Information derived from the TXM-XANES will contribute to design of electrode materials, such as electrode with porous structures, to acquire reversible electrochemical properties. X-ray nanotomography, in-situ XRD, and electrochemical impedance spectroscopy (EIS) were also involved in this work to resolve the irreversible capacity and morphology variations of the metal sulfides. This study proves the microstructure evolution, intrinsic Na-ion slow diffusion kinetics and two-phase interface slow mobility of ions contribute collaboratively to the higher irreversible capacity during the first cycle and will guide the conversion reaction material design to achieve preferred electrochemical activity and stability.

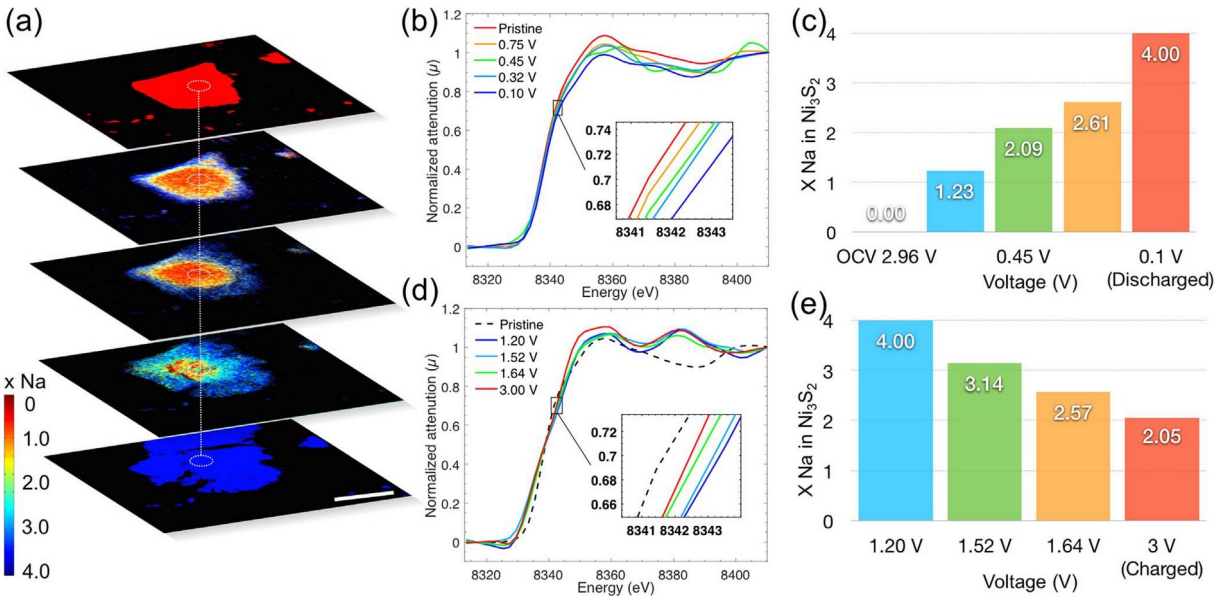

Figure 16. Quantification analysis of the selected area for the first cycle. (a) Selected area of the 2D TXM-XANES chemical phase mappings during sodiation process. Scale bar: 10 μm. (b) The average XANES spectra at selected states and (c) corresponding to Na ions content in per cell unit in the first discharge process. (d) The average XANES spectra at selected states and (e) corresponding to Na ion content per cell unit in the first charge process. Reproduced with permission.[15] Copyright 2018 Elsevier.

Compared to that of Li^+, the radius of Na^+ is larger, thus the currently used Li-ion battery anode is not suitable for Na-ion batteries.[107] To address this issue, 2D transition metal carbides and nitrides, known as MXenes, is catching lots of attention because of their high electrical conductivity, good stability and large redox-active surface area.[108] As an example, in the probing of the charge storage mechanism of a 2D vanadium carbide MXene, V_2CT_x, where T_x are surface functional group, both hard and soft X-ray absorption spectroscopic methods are used.[14] The XANES of V K-edge measured by hard X-ray exhibits a weak pre-edge peak at 5470 eV and a strong main absorption peak at 5485 eV, corresponding to the transition of one 1s electron to the hybridized t_{2g} and e_g orbitals, and the dipole allowed

transition of 1s electrons to unoccupied V 4p states, respectively. This V K-edge XANES indicates the redox reaction at the transition metal site in MXene is accountable for electrochemical charge storage. Soft X-ray absorption spectroscopy makes it more convincing by a direct probe of the dipole allowed 2p-3d transition of the transition metal. The CO_3^{2-} content is correlated with the Na^+ intercalation/deintercalation in the V_2CT_x electrode. Implied by the C and O K-edge XAS, some additional charge storage reactions may take place, however this is not fully understood yet, but the information derived from both hard and soft XAS are valuable for future Na-ion battery/capacitor anode material studies. Many additional work reported in recent years in the Na-ion battery research in both anode[12] and cathode[13] materials involve with (soft) XAS.

Similarly, potassium (K) battery received lots of attention for their application in energy storage because of the abundance of K and its promising intercalation chemistries with graphite.[109] Nevertheless, accommodating the large size of K^+ ions requires the development of suitable cathode materials, which is usually achieved through designing nanostructures, increasing crystallinity, using carbon as matrixes for conductivity, optimizing electrolytes, etc.[110] In such studies, both XANES and EXAFS together with other X-ray techniques such as X-ray diffraction (XRD) are used to divulge the valency and the local chemical structures. [111,112]

3. Other in-situ/operando (soft) X-ray spectroscopy techniques

In section 2.3 regarding the involvement of (soft) X-ray absorption spectroscopy in the study of Na-ion batteries, transmission X-ray microscopy (TXM) as an additional X-ray technique, has been introduced. Here in this section, a few examples of using resonant inelastic X-ray scattering (RIXS) in the investigation of beyond lithium-ion batteries will be presented.

RIXS, together with XAS and XES, belongs to the core-level X-ray spectroscopy which involves the excitation of core-level electrons of an element of interest.[61] XAS, XES and RIXS are relevant to decay processes after the excitation, which corresponds to the unoccupied states, occupied states, and detailed band structure and low excitations, respectively.[63] RIXS with the capability to distinguish the same element with inequivalent chemical environment is ideal to deal with electronic band structure and elementary excitations. It has been used in the investigation of various battery systems, such as the monovalent manganese for sodium-ion batteries[16], the phase transitions in the magnesium-sulfur batteries[113], and the chemical state of oxygen in cathode systems with active oxygen redox reactions.[114,115] Spectroscopic studies regarding O_2 based on oxygen K-edge XAS and RIXS at particular excitation energies have been studied since decades ago.[116–118] While these investigations show interesting results on vibrational coupling, Yang and coworkers reported the oxidized oxygen displays two characteristic features in mapping of RIXS (mRIXS).[119] Such mRIXS across a wide range of energy range of both excitation and emission energies is crucial in the investigation of nondivalent oxygen states. For example, figure 17 provides a direct comparison of the full energy range O-K mRIXS results collected from gas phase O_2, Li_2O_2, and the oxidized oxygen state in both Li-ion and Na-ion battery electrodes.[65] The direct mRIXS comparison between the solid samples and gas phase reference shows the general similarity of the oxidized oxygen states, however, indicates the different nature of the states in the molecular systems and the transition-metal oxide electrodes.[120] The oxygen redox states in batteries show distinct widths and positions along the excitation energy compared to Li_2O_2 and O_2. The full mRIXS profile indicates varying distributions of these oxidized oxygen features along excitation energies, Li_2O_2 shows the longest distribution and O_2 has the shortest, with a color scale showing the same emission energy expansion. Thus, the oxidized oxygen state nature in such oxide electrodes is beyond a simple molecular

configuration of O_2 or peroxide. This work clarifies some speculations regarding the oxidized oxygen state while a systematic understanding of such oxygen redox is still undergoing and requires more efforts in the fundamental physics perspective.

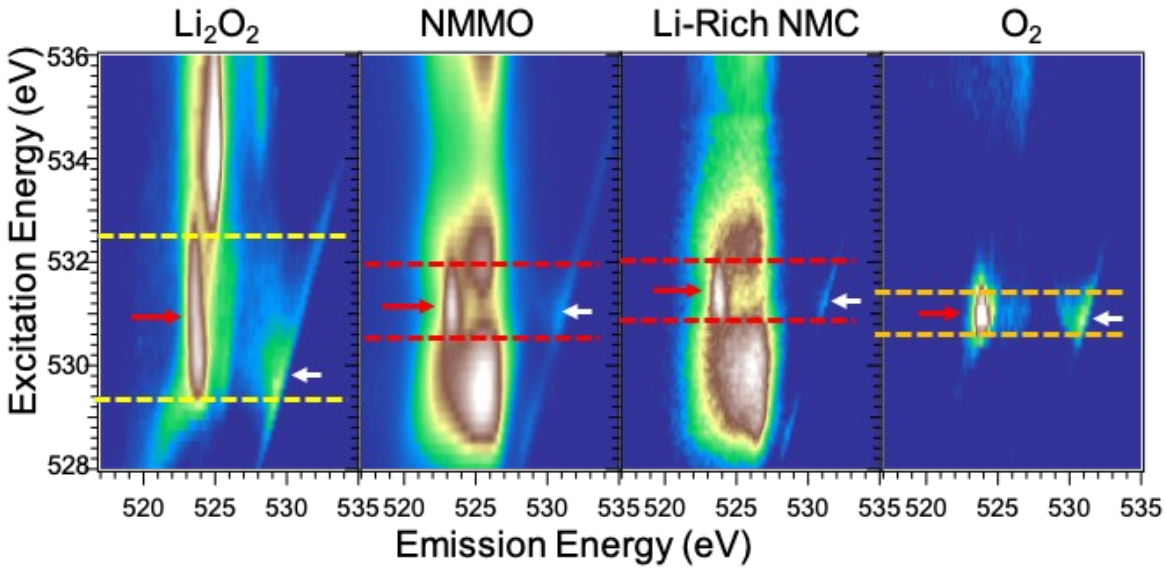

Figure 17. Mapping of RIXS (mRIXS) profile of oxidized oxygen states in Li_2O_2, charged NMMO ($Na_{2/3}Mg_{1/3}Mn_{2/3}O_2$), Li-rich NMC and O_2. Reproduced with permission.[120] Copyright 2020 American Chemical Society.

4. Perspectives of in-situ/operando X-ray spectroscopy in beyond lithium-ion batteries

Considering the cost, safety, energy density, cycling life and abundance, beyond lithium-ion batteries are of primary interest to meet "the challenge in the design of an electrochemical technology that can perform safely the task of electrical-energy storage and recovery at a rate and cost that are competitive with the performance of the well-established fossil fuel technologies", from a perspective of the battery pioneer J. B. Goodenough.[121] In

this article, we have reviewed the application of in-situ/operando (soft) X-ray spectroscopies, including (soft) XAS and other techniques such as TXM, and RIXS in the advancing of our knowledge in various beyond lithium-ion batteries. The development of in-situ/operando experimental setup will also shed more light on the transient interfacial processes. A new beamline here at ALS, Advanced Materials Beamline for Energy Research (AMBER), is about to become available which will be dedicated for in-situ/operando soft X-ray spectroscopies including XAS, XES and RIXS to allow the study of surfaces, interfaces and bulk electronic structure of novel energy storage materials.[122]

Being part of the Joint Center for Energy Storage Research (JCESR), our goal is to attain a unified understanding of the ion solvation and its variation at the atomic level, through which the ion solubility, reactivity and stability can be regulated in a controlled manner, leading to breakthroughs in energy storage science. To solve the questions in remain such as calcium solvation, charge transfer at electrolyte/electrode interfaces, these cutting-edge in-situ/operando (soft) X-ray spectroscopy techniques will play the irreplaceable role while their unique capabilities will also benefit a broader science community.

Acknowledgments

This work was supported as part of the Joint Center for Energy Storage Research (JCESR), an Energy Innovation Hub funded by the U.S. Department of Energy (DOE), Office of Science, Basic Energy Sciences. The soft XAS and RIXS experiments are performed on the beamlines 6.3.1.2, 7.3.1 and 8.0.1. This research used resources of the Advanced Light Source, a U.S. DOE Office of Science User Facility under contract no. DE-AC02-05CH11231.

References

[1] M. Li, J. Lu, Z. Chen, K. Amine, *Adv. Mater.* **2018**, *30*, 1800561.

[2] M. Armand, J. M. Tarascon, *Nature* **2008**, *451*, 652.

[3] N. Nitta, F. Wu, J. T. Lee, G. Yushin, *Mater. Today* **2015**, *18*, 252.

[4] A. Luntz, *J. Phys. Chem. Lett.* **2015**, *6*, 300.

[5] J. Biemolt, P. Jungbacker, T. van Teijlingen, N. Yan, G. Rothenberg, *Materials (Basel).* **2020**, *13*, 425.

[6] J. M. Tarascon, M. Armand, *Nature* **2001**, *414*, 359.

[7] P. G. Bruce, S. A. Freunberger, L. J. Hardwick, J. M. Tarascon, *Nat. Mater.* **2012**, *11*, 19.

[8] J. W. Choi, D. Aurbach, *Nat. Rev. Mater.* **2016**, *1*, 16013.

[9] A. C. Luntz, B. D. McCloskey, *Chem. Rev.* **2014**, *114*, 11721.

[10] L. Zhang, J. Guo, *Arab. J. Sci. Eng.* **2019**, *44*, 6217.

[11] M. Cuisinier, C. Hart, M. Balasubramanian, A. Garsuch, L. F. Nazar, *Adv. Energy Mater.* **2015**, *5*, 1401801.

[12] K. Zhang, M. Park, L. Zhou, G.-H. Lee, J. Shin, Z. Hu, S.-L. Chou, J. Chen, Y.-M. Kang, *Angew. Chemie* **2016**, *128*, 13014.

[13] K. W. Nam, S. Kim, E. Yang, Y. Jung, E. Levi, D. Aurbach, J. W. Choi, *Chem. Mater.* **2015**, *27*, 3721.

[14] S. M. Bak, R. Qiao, W. Yang, S. Lee, X. Yu, B. Anasori, H. Lee, Y. Gogotsi, X. Q. Yang, *Adv. Energy Mater.* **2017**, *7*, 1700959.

[15] L. Wang, J. Wang, F. Guo, L. Ma, Y. Ren, T. Wu, P. Zuo, G. Yin, J. Wang, *Nano Energy* **2018**, *43*, 184.

[16] A. Firouzi, R. Qiao, S. Motallebi, C. W. Valencia, H. S. Israel, M. Fujimoto, L. A.

Wray, Y. De Chuang, W. Yang, C. D. Wessells, *Nat. Commun.* **2018**, *9*, 861.

[17] N. T. Hahn, J. Self, T. J. Seguin, D. M. Driscoll, M. A. Rodriguez, M. Balasubramanian, K. A. Persson, K. R. Zavadil, *J. Mater. Chem. A* **2020**, *8*, 7235.

[18] T. S. Arthur, P.-A. Glans, N. Singh, O. Tutusaus, K. Nie, Y.-S. Liu, F. Mizuno, J. Guo, D. H. Alsem, N. J. Salmon, R. Mohtadi, *Chem. Mater.* **2017**, *29*, 7183.

[19] R. Zhang, X. Yu, K. W. Nam, C. Ling, T. S. Arthur, W. Song, A. M. Knapp, S. N. Ehrlich, X. Q. Yang, M. Matsui, *Electrochem. commun.* **2012**, *23*, 110.

[20] A. Watanabe, K. Yamamoto, Y. Orikasa, T. Masese, T. Mori, T. Uchiyama, T. Matsunaga, Y. Uchimoto, *Solid State Ionics* **2020**, *349*, 115311.

[21] Y. Orikasa, T. Masese, Y. Koyama, T. Mori, M. Hattori, K. Yamamoto, T. Okado, Z. D. Huang, T. Minato, C. Tassel, J. Kim, Y. Kobayashi, T. Abe, H. Kageyama, Y. Uchimoto, *Sci. Rep.* **2014**, *4*, 5622.

[22] H. Wang, X. Feng, Y. Chen, Y. S. Liu, K. S. Han, M. Zhou, M. H. Engelhard, V. Murugesan, R. S. Assary, T. L. Liu, W. Henderson, Z. Nie, M. Gu, J. Xiao, C. Wang, K. Persson, D. Mei, J. G. Zhang, K. T. Mueller, J. Guo, K. Zavadil, Y. Shao, J. Liu, *ACS Energy Lett.* **2020**, *5*, 200.

[23] H. D. Yoo, Y. Liang, H. Dong, J. Lin, H. Wang, Y. Liu, L. Ma, T. Wu, Y. Li, Q. Ru, Y. Jing, Q. An, W. Zhou, J. Guo, J. Lu, S. T. Pantelides, X. Qian, Y. Yao, *Nat. Commun.* **2017**, *8*, 339.

[24] T. Mori, T. Masese, Y. Orikasa, Z. D. Huang, T. Okado, J. Kim, Y. Uchimoto, *Phys. Chem. Chem. Phys.* **2016**, *18*, 13524.

[25] J. Han, S. Yagi, T. Ichitsubo, *J. Power Sources* **2019**, *435*, 226822.

[26] N. Sa, H. Wang, D. L. Proffit, A. L. Lipson, B. Key, M. Liu, Z. Feng, T. T. Fister, Y. Ren, C. J. Sun, J. T. Vaughey, P. A. Fenter, K. A. Persson, A. K. Burrell, *J. Power*

Sources **2016**, *323*, 44.

[27] T. S. Arthur, N. Singh, M. Matsui, *Electrochem. commun.* **2012**, *16*, 103.

[28] K. Shimokawa, T. Atsumi, M. Harada, R. E. Ward, M. Nakayama, Y. Kumagai, F. Oba, N. L. Okamoto, K. Kanamura, T. Ichitsubo, *J. Mater. Chem. A* **2019**, *7*, 12225.

[29] T. S. Arthur, K. Kato, J. Germain, J. Guo, P.-A. Glans, Y.-S. Liu, D. Holmes, X. Fan, F. Mizuno, *Chem. Commun.* **2015**, *51*, 15657.

[30] Y. Li, Q. An, Y. Cheng, Y. Liang, Y. Ren, C. J. Sun, H. Dong, Z. Tang, G. Li, Y. Yao, *Nano Energy* **2017**, *34*, 188.

[31] Q. D. Truong, M. K. Devaraju, I. Honma, *J. Power Sources* **2017**, *361*, 195.

[32] F. Mizuno, N. Singh, T. S. Arthur, P. T. Fanson, M. Ramanathan, A. Benmayza, J. Prakash, Y. S. Liu, P. A. Glans, J. Guo, *Front. Energy Res.* **2014**, *2*, 46.

[33] T. S. Arthur, R. Zhang, C. Ling, P.-A. Glans, X. Fan, J. Guo, F. Mizuno, *ACS Appl. Mater. Interfaces* **2014**, *6*, 7004.

[34] A. Benmayza, M. Ramanathan, T. S. Arthur, M. Matsui, F. Mizuno, J. Guo, P.-A. Glans, J. Prakash, *J. Phys. Chem. C* **2013**, *117*, 26881.

[35] T. S. Arthur, P.-A. Glans, M. Matsui, R. Zhang, B. Ma, J. Guo, *Electrochem. commun.* **2012**, *24*, 43.

[36] A. L. Lipson, S. D. Han, S. Kim, B. Pan, N. Sa, C. Liao, T. T. Fister, A. K. Burrell, J. T. Vaughey, B. J. Ingram, *J. Power Sources* **2016**, *325*, 646.

[37] Y. Xu, G. Zhou, S. Zhao, W. Li, F. Shi, J. Li, J. Feng, Y. Zhao, Y. Wu, J. Guo, Y. Cui, Y. Zhang, *Adv. Sci.* **2019**, *6*, 1800981.

[38] Y. Orikasa, K. Kisu, E. Iwama, W. Naoi, Y. Yamaguchi, Y. Yamaguchi, N. Okita, K. Ohara, T. Munesada, M. Hattori, K. Yamamoto, P. Rozier, P. Simon, K. Naoi, *Chem. Mater.* **2020**, *32*, 1011.

[39] P. Senguttuvan, S. D. Han, S. Kim, A. L. Lipson, S. Tepavcevic, T. T. Fister, I. D. Bloom, A. K. Burrell, C. S. Johnson, *Adv. Energy Mater.* **2016**, *6*, 1600826.

[40] Q. Yang, Y. Guo, B. Yan, C. Wang, Z. Liu, Z. Huang, Y. Wang, Y. Li, H. Li, L. Song, J. Fan, C. Zhi, *Adv. Mater.* **2020**, 2001755.

[41] A. El Kharbachi, O. Zavorotynska, M. Latroche, F. Cuevas, V. Yartys, M. Fichtner, *J. Alloys Compd.* **2020**, *817*, 153261.

[42] N. Yabuuchi, K. Kubota, M. Dahbi, S. Komaba, *Chem. Rev.* **2014**, *114*, 11636.

[43] J. Park, Z.-L. Xu, K. Kang, *Front. Chem.* **2020**, *8*, 432.

[44] D. Aurbach, Z. Lu, A. Schechter, Y. Gofer, H. Gizbar, R. Turgeman, Y. Cohen, M. Moshkovich, E. Levi, *Nature* **2000**, *407*, 724.

[45] C. Xu, B. Li, H. Du, F. Kang, *Angew. Chemie - Int. Ed.* **2012**, *51*, 933.

[46] F. Cheng, J. Chen, X. Gou, P. Shen, *Adv. Mater.* **2005**, *17*, 2753.

[47] J. B. Goodenough, K. S. Park, *J. Am. Chem. Soc.* **2013**, *135*, 1167.

[48] A. Ponrouch, R. Dedryvère, D. Monti, A. E. Demet, J. M. Ateba Mba, L. Croguennec, C. Masquelier, P. Johansson, M. R. Palacín, *Energy Environ. Sci.* **2013**, *6*, 2361.

[49] M. Sawicki, L. L. Shaw, *RSC Adv.* **2015**, *5*, 53129.

[50] L. G. Chagas, D. Buchholz, L. Wu, B. Vortmann, S. Passerini, *J. Power Sources* **2014**, *247*, 377.

[51] N. Naveen, W. B. Park, S. C. Han, S. P. Singh, Y. H. Jung, D. Ahn, K. S. Sohn, M. Pyo, *Chem. Mater.* **2018**, *30*, 2049.

[52] H. Yaghoobnejad Asl, J. Fu, H. Kumar, S. S. Welborn, V. B. Shenoy, E. Detsi, *Chem. Mater.* **2018**, *30*, 1815.

[53] S. Wu, F. Zhang, Y. Tang, *Adv. Sci.* **2018**, *5*, 1701082.

[54] A. L. Lipson, S. Kim, B. Pan, C. Liao, T. T. Fister, B. J. Ingram, *J. Power Sources*

2017, *369*, 133.

[55] M. Adil, A. Sarkar, A. Roy, M. R. Panda, A. Nagendra, S. Mitra, *ACS Appl. Mater. Interfaces* **2020**, *12*, 11489.

[56] N. Zhang, Y. Dong, M. Jia, X. Bian, Y. Wang, M. Qiu, J. Xu, Y. Liu, L. Jiao, F. Cheng, *ACS Energy Lett.* **2018**, *3*, 1366.

[57] L. Ma, N. Li, C. Long, B. Dong, D. Fang, Z. Liu, Y. Zhao, X. Li, J. Fan, S. Chen, S. Zhang, C. Zhi, *Adv. Funct. Mater.* **2019**, *29*, 1906142.

[58] S. M. Bak, Z. Shadike, R. Lin, X. Yu, X. Q. Yang, *NPG Asia Mater.* **2018**, *10*, 563.

[59] W. Li, M. Li, Y. Hu, J. Lu, A. Lushington, R. Li, T. Wu, T.-K. Sham, X. Sun, *Small Methods* **2018**, *2*, 1700341.

[60] S. Yang, D. Wang, G. Liang, Y. M. Yiu, J. Wang, L. Liu, X. Sun, T. K. Sham, *Energy Environ. Sci.* **2012**, *5*, 7007.

[61] F. Lin, Y. Liu, X. Yu, L. Cheng, A. Singer, O. G. Shpyrko, H. L. Xin, N. Tamura, C. Tian, T.-C. Weng, X.-Q. Yang, Y. S. Meng, D. Nordlund, W. Yang, M. M. Doeff, *Chem. Rev.* **2017**, *117*, 13123.

[62] P. P. R. M. L. Harks, F. M. Mulder, P. H. L. Notten, *J. Power Sources* **2015**, *288*, 92.

[63] X. Liu, W. Yang, Z. Liu, *Adv. Mater.* **2014**, *26*, 7710.

[64] L. J. P. Ament, M. Van Veenendaal, T. P. Devereaux, J. P. Hill, J. Van Den Brink, *Rev. Mod. Phys.* **2011**, *83*, 705.

[65] K. Dai, J. Wu, Z. Zhuo, Q. Li, S. Sallis, J. Mao, G. Ai, C. Sun, Z. Li, W. E. Gent, W. C. Chueh, Y. de Chuang, R. Zeng, Z. xun Shen, F. Pan, S. Yan, L. F. J. Piper, Z. Hussain, G. Liu, W. Yang, *Joule* **2019**, *3*, 518.

[66] K. Dai, J. Mao, Z. Zhuo, Y. Feng, W. Mao, G. Ai, F. Pan, Y. de Chuang, G. Liu, W. Yang, *Nano Energy* **2020**, *74*, 104831.

[67] Q. Li, R. Qiao, L. A. Wray, J. Chen, Z. Zhuo, Y. Chen, S. Yan, F. Pan, Z. Hussain, W. Yang, *J. Phys. D. Appl. Phys.* **2016**, *49*, 413003.

[68] W. Yang, X. Liu, R. Qiao, P. Olalde-Velasco, J. D. Spear, L. Roseguo, J. X. Pepper, Y. De Chuang, J. D. Denlinger, Z. Hussain, *J. Electron Spectros. Relat. Phenomena* **2013**, *190*, 64.

[69] J. J. Rehr, J. J. Kas, M. P. Prange, A. P. Sorini, Y. Takimoto, F. Vila, *Comptes Rendus Phys.* **2009**, *10*, 548.

[70] M. Wu, X. Xiao, N. Vukmirovic, S. Xun, P. K. Das, X. Song, P. Olalde-Velasco, D. Wang, A. Z. Weber, L. W. Wang, V. S. Battaglia, W. Yang, G. Liu, *J. Am. Chem. Soc.* **2013**, *135*, 12048.

[71] W. Yang, in *Encycl. Inorg. Bioinorg. Chem.*, John Wiley & Sons, Ltd, Chichester, UK, **2019**, pp. 1–18.

[72] Y. L. Jeyachandran, F. Meyer, S. Nagarajan, A. Benkert, M. Bär, M. Blum, W. Yang, F. Reinert, C. Heske, L. Weinhardt, M. Zharnikov, *J. Phys. Chem. Lett.* **2014**, *5*, 4143.

[73] X. Liu, D. Wang, G. Liu, V. Srinivasan, Z. Liu, Z. Hussain, W. Yang, *Nat. Commun.* **2013**, *4*, DOI 10.1038/ncomms3568.

[74] P. Jiang, J. L. Chen, F. Borondics, P. A. Glans, M. W. West, C. L. Chang, M. Salmeron, J. Guo, *Electrochem. commun.* **2010**, *12*, 820.

[75] J. Guo, T. Tong, L. Svec, J. Go, C. Dong, J.-W. Chiou, *J. Vac. Sci. Technol. A Vacuum, Surfaces, Film.* **2007**, *25*, 1231.

[76] Y. S. Liu, P. A. Glans, C. H. Chuang, M. Kapilashrami, J. Guo, *J. Electron Spectros. Relat. Phenomena* **2015**, *200*, 282.

[77] Y. Li, Y. Lu, C. Zhao, Y. S. Hu, M. M. Titirici, H. Li, X. Huang, L. Chen, *Energy Storage Mater.* **2017**, *7*, 130.

[78] C. Liebenow, *J. Appl. Electrochem.* **1997**, *27*, 221.

[79] J. H. Connor, W. E. Reid, G. B. Wood, *J. Electrochem. Soc.* **1957**, *104*, 38.

[80] H. D. Yoo, I. Shterenberg, Y. Gofer, G. Gershinsky, N. Pour, D. Aurbach, *Energy Environ. Sci.* **2013**, *6*, 2265.

[81] M. Matsui, *J. Power Sources* **2011**, *196*, 7048.

[82] F. Liu, T. Wang, X. Liu, L. Fan, *Adv. Energy Mater.* **2020**, 2000787.

[83] R. Mohtadi, M. Matsui, T. S. Arthur, S. J. Hwang, *Angew. Chemie - Int. Ed.* **2012**, *51*, 9780.

[84] J. Muldoon, C. B. Bucur, A. G. Oliver, T. Sugimoto, M. Matsui, H. S. Kim, G. D. Allred, J. Zajicek, Y. Kotani, *Energy Environ. Sci.* **2012**, *5*, 5941.

[85] Y. Shao, T. Liu, G. Li, M. Gu, Z. Nie, M. Engelhard, J. Xiao, D. Lv, C. Wang, J. G. Zhang, J. Liu, *Sci. Rep.* **2013**, *3*, 3130.

[86] O. Tutusaus, R. Mohtadi, T. S. Arthur, F. Mizuno, E. G. Nelson, Y. V. Sevryugina, *Angew. Chemie - Int. Ed.* **2015**, *54*, 7900.

[87] L. C. Kao, X. Feng, Y. Ha, F. Yang, Y.-S. Liu, N. T. Hahn, J. MacDougall, W. Chao, W. Yang, K. R. Zavadil, J. Guo, *Surf. Sci.* **2020**, *702*, 121720.

[88] Q. Fu, A. Sarapulova, V. Trouillet, L. Zhu, F. Fauth, S. Mangold, E. Welter, S. Indris, M. Knapp, S. Dsoke, N. Bramnik, H. Ehrenberg, *J. Am. Chem. Soc.* **2019**, *141*, 2305.

[89] J. Han, S. Yagi, T. Ichitsubo, *J. Power Sources* **2019**, *435*, 226822.

[90] L. F. Wan, J. Wright, B. R. Perdue, T. T. Fister, S. Kim, C. A. Apblett, D. Prendergast, *Phys. Chem. Chem. Phys.* **2016**, *18*, 17326.

[91] R. Zhang, X. Yu, K. W. Nam, C. Ling, T. S. Arthur, W. Song, A. M. Knapp, S. N. Ehrlich, X. Q. Yang, M. Matsui, *Electrochem. commun.* **2012**, *23*, 110.

[92] M. S. Islam, D. J. Driscoll, C. A. J. Fisher, P. R. Slater, *Chem. Mater.* **2005**, *17*, 5085.

[93] S. I. Nishimura, G. Kobayashi, K. Ohoyama, R. Kanno, M. Yashima, A. Yamada, *Nat. Mater.* **2008**, *7*, 707.

[94] T. Mori, T. Masese, Y. Orikasa, Z. D. Huang, T. Okado, J. Kim, Y. Uchimoto, *Phys. Chem. Chem. Phys.* **2016**, *18*, 13524.

[95] A. Watanabe, K. Yamamoto, Y. Orikasa, T. Masese, T. Mori, T. Uchiyama, T. Matsunaga, Y. Uchimoto, *Solid State Ionics* **2020**, *349*, 115311.

[96] Y. Orikasa, K. Kisu, E. Iwama, W. Naoi, Y. Yamaguchi, Y. Yamaguchi, N. Okita, K. Ohara, T. Munesada, M. Hattori, K. Yamamoto, P. Rozier, P. Simon, K. Naoi, *Chem. Mater.* **2020**, *32*, 1011.

[97] A. Deb, U. Bergmann, E. J. Cairns, S. P. Cramer, *J. Synchrotron Radiat.* **2004**, *11*, 497.

[98] K. I. Pandya, *J. Electrochem. Soc.* **1990**, *137*, 383.

[99] A. Bianconi, M. Dell'Ariccia, P. J. Durham, J. B. Pendry, *Phys. Rev. B* **1982**, *26*, 6502.

[100] Y. Shao, M. Gu, X. Li, Z. Nie, P. Zuo, G. Li, T. Liu, J. Xiao, Y. Cheng, C. Wang, J.-G. Zhang, J. Liu, *Nano Lett.* **2014**, *14*, 255.

[101] D. Kundu, B. D. Adams, V. Duffort, S. H. Vajargah, L. F. Nazar, *Nat. Energy* **2016**, *1*, 16119.

[102] J. Wong, F. W. Lytle, R. P. Messmer, D. H. Maylotte, *Phys. Rev. B* **1984**, *30*, 5596.

[103] A. L. Lipson, S. Kim, B. Pan, C. Liao, T. T. Fister, B. J. Ingram, *J. Power Sources* **2017**, *369*, 133.

[104] D. Wang, X. Gao, Y. Chen, L. Jin, C. Kuss, P. G. Bruce, *Nat. Mater.* **2018**, *17*, 16.

[105] F. Yang, Y.-S. Liu, X. Feng, K. Qian, L. C. Kao, Y. Ha, N. T. Hahn, T. J. Seguin, M. Tsige, W. Yang, K. R. Zavadil, K. A. Persson, J. Guo, *RSC Adv.* **2020**, *10*, 27315.

[106] J. Wang, X. Sun, *Energy Environ. Sci.* **2012**, *5*, 5163.

[107] S. W. Kim, D. H. Seo, X. Ma, G. Ceder, K. Kang, *Adv. Energy Mater.* **2012**, *2*, 710.

[108] M. Naguib, J. Halim, J. Lu, K. M. Cook, L. Hultman, Y. Gogotsi, M. W. Barsoum, *J. Am. Chem. Soc.* **2013**, *135*, 15966.

[109] Q. Zhang, Z. Wang, S. Zhang, T. Zhou, J. Mao, Z. Guo, *Electrochem. Energy Rev.* **2018**, *1*, 625.

[110] C. D. Wessells, S. V. Peddada, R. A. Huggins, Y. Cui, *Nano Lett.* **2011**, *11*, 5421.

[111] B. Ji, W. Yao, Y. Zheng, P. Kidkhunthod, X. Zhou, S. Tunmee, S. Sattayaporn, H. M. Cheng, H. He, Y. Tang, *Nat. Commun.* **2020**, *11*, 1225.

[112] T. Masese, K. Yoshii, Y. Yamaguchi, T. Okumura, Z. D. Huang, M. Kato, K. Kubota, J. Furutani, Y. Orikasa, H. Senoh, H. Sakaebe, M. Shikano, *Nat. Commun.* **2018**, *9*, 3823.

[113] A. Robba, A. Vizintin, J. Bitenc, G. Mali, I. Arčon, M. Kavčič, M. Žitnik, K. Bučar, G. Aquilanti, C. Martineau-Corcos, A. Randon-Vitanova, R. Dominko, *Chem. Mater.* **2017**, *29*, 9555.

[114] A. Grimaud, W. T. Hong, Y. Shao-Horn, J. M. Tarascon, *Nat. Mater.* **2016**, *15*, 121.

[115] J. Wu, Z. Zhuo, X. Rong, K. Dai, Z. Lebens-Higgins, S. Sallis, F. Pan, L. F. J. Piper, G. Liu, Y. de Chuang, Z. Hussain, Q. Li, R. Zeng, Z. xun Shen, W. Yang, *Sci. Adv.* **2020**, *6*, eaaw3871.

[116] P. Glans, K. Gunnelin, P. Skytt, J. H. Guo, N. Wassdahl, J. Nordgren, M. Ågren, F. K. Gel'mukhanov, T. Warwick, E. Rotenberg, *Phys. Rev. Lett.* **1996**, *76*, 2448.

[117] A. Cesar, F. Gel'mukhanov, Y. Luo, H. Ågren, P. Skytt, P. Glans, J. Guo, K. Gunnelin, J. Nordgren, *J. Chem. Phys.* **1997**, *106*, 3439.

[118] F. Hennies, A. Pietzsch, M. Berglund, A. Föhlisch, T. Schmitt, V. Strocov, H. O. Karlsson, J. Andersson, J. E. Rubensson, *Phys. Rev. Lett.* **2010**, *104*, 193002.

[119] J. Wu, Q. Li, S. Sallis, Z. Zhuo, W. E. Gent, W. C. Chueh, S. Yan, Y. Chuang, W.

Yang, *Condens. Matter* **2019**, *4*, 5.

[120] Z. Zhuo, Y. S. Liu, J. Guo, Y. De Chuang, F. Pan, W. Yang, *J. Phys. Chem. Lett.* **2020**, *11*, 2618.

[121] J. B. Goodenough, *Energy Storage Mater.* **2015**, *1*, 158.

[122] P. A. Glans, Y. S. Liu, E. Crumlin, W. Yang, T. Warwick, Z. Hussain, J. Guo, *Synchrotron Radiat. News* **2017**, *30*, 41.

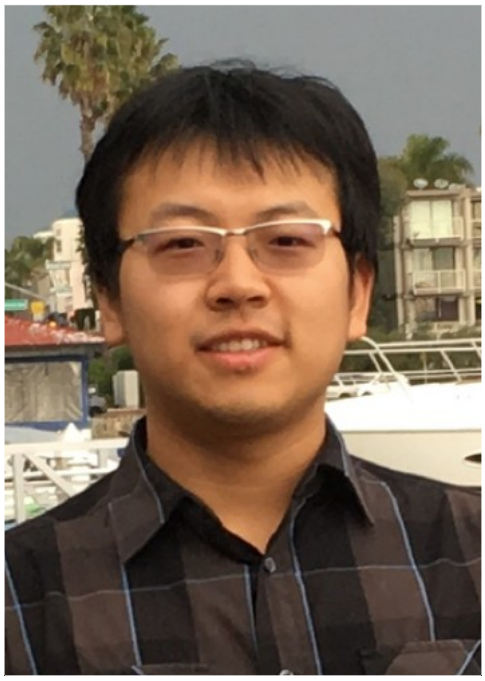

Feipeng Yang is a postdoctoral fellow in the group of Dr. Jinghua Guo at Advanced Light Source, Lawrence Berkeley National Laboratory performing soft X-ray spectroscopic studies on energy materials as part of the Joint Center for Energy Storage Research (JCESR) Hub. He obtained his Ph.D. degree from The Department of Polymer Science, The University of Akron in 2018. He is dedicated in using in-situ/operando soft X-ray core-level spectroscopies to study the electronic structure of beyond lithium-ion battery materials and participating in planning and implementation of upgrades of the in-situ soft X-ray spectroscopy cells.

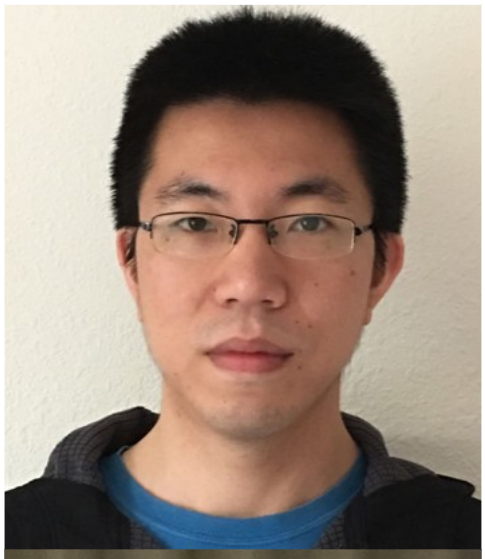

Xuefei Feng obtained his Ph.D. degree from University of Science and Technology of China in 2014. After two years of postdoc fellow in Shanghai Institute of Microsystem and Information Technology, CAS., he joined in the group of Dr. Jinghua Guo at Advanced Light Source, Lawrence Berkeley National Laboratory as a postdoc in 2016. He is now a project scientist as part of the Joint Center for Energy Storage Research (JCESR) Hub. His research interest is scientific instrument development for in-situ/operando soft X-ray spectroscopic study on energy materials.

Yi-Sheng Liu is a project scientist at the Advanced Light Source, Lawrence Berkeley National Laboratory. His research interest is in studying energy materials through in-situ and ex-situ soft X-ray spectroscopies.

He is also dedicated to the development of in-situ soft X-ray capabilities applied to energy materials especially for metal ion batteries and hydrogen storage.

Li Cheng Kao is a postdoctoral research fellow at Advanced Light Source, Lawrence Berkeley National Laboratory. He is enthusiastic about discovering the opportunities for synchrotron-based investigations in the environment and energy sciences to advance strategic science areas. He also dedicates to the new sample deliver method and probing technique of liquid phase in ultra-high vacuum system.

Per-Anders Glans is a Research Scientist at the Advanced Light Source, Lawrence Berkeley National Laboratory. He has experience with photoemission, as well as photon-in, photon-out techniques such as soft X-ray absorption, soft X-ray emission, and resonant

inelastic X-ray scattering. He is currently building a high-resolution soft X-ray beamline with associated X-ray emission spectrometer.

Wanli Yang is a staff scientist at the Advanced Light Source of Lawrence Berkeley National Laboratory. His research interest focuses on soft x-ray spectroscopy of electrochemical materials. He has recently led the efforts on high efficiency resonant inelastic x-ray scattering (RIXS) for practical material researches, especially for detecting the evolving chemical states of both transition metals and oxygen in battery electrodes.

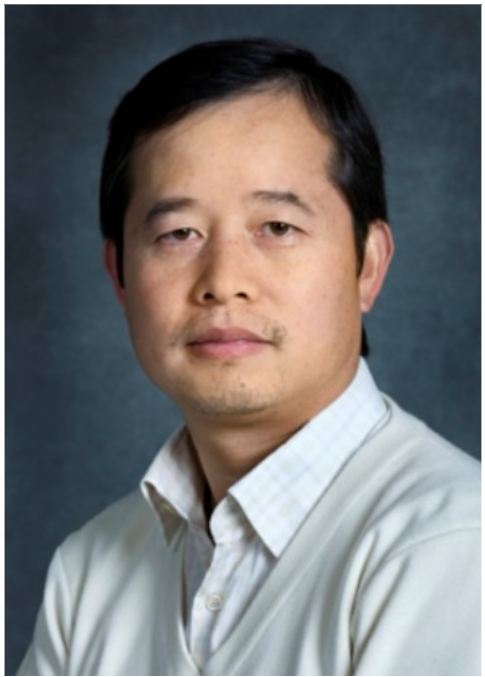

Jinghua Guo is a Senior Scientist and RIXS Program Lead

at Advanced Light Source, Lawrence Berkeley National Laboratory, an adjunct professor in the Department of Chemistry and Biochemistry, University of California at Santa Cruz, and a Fellow of American Physical Society. His research on soft X-ray spectroscopic characterization techniques has recently been honored with the Materials Research Society (MRS) Innovation in Materials Characterization Award “for pioneering in situ/operando soft X-ray spectroscopy characterization of interfacial phenomena in energy, catalysis and chemical materials science.” He has published over 400 peer-reviewed articles with more than 23700 citations.